

---

MASTER PROJECT

---

# ELECTRO-MECHANICAL MODELLING OF DYNAMIC LOUDSPEAKERS

---

conducted at the  
Signal Processing and Speech Communications Laboratory  
Graz University of Technology, Austria

by  
Markus Faymann, BSc

Supervisor:  
Dipl.-Ing. Dr.techn. Werner Weselak

# Contents

<b>1</b>	<b>Introduction</b>	<b>1</b>
<b>2</b>	<b>Voice coil impedance modelling</b>	<b>2</b>
2.1	L2R . . . . .	2
2.2	L3R . . . . .	3
2.3	L2RK . . . . .	5
2.4	Leach . . . . .	7
2.5	Wright . . . . .	8
<b>3</b>	<b>Suspension creep modelling</b>	<b>9</b>
3.1	Standard linear solid model . . . . .	10
3.2	Complex logarithmic model by Knudsen . . . . .	12
3.3	Simplified logarithmic model by Knudsen . . . . .	14
3.4	Logarithmic models by Ritter . . . . .	16
3.4.1	Three parameter model . . . . .	17
3.4.2	Four parameter model . . . . .	18
<b>4</b>	<b>Measurements and evaluation of the advanced models</b>	<b>20</b>
4.1	Overview . . . . .	20
4.2	Measurement and simulation procedure . . . . .	22
4.3	Measurement results in free air . . . . .	24
<b>5</b>	<b>Simulation Program</b>	<b>30</b>
5.1	Voice Coil Parameters . . . . .	31
5.2	Suspension Creep Parameters . . . . .	31
<b>A</b>	<b>Measurement data and source code</b>	<b>33</b>

## 1

## Introduction

As the demand for high-quality dynamic loudspeaker systems rises, accurate models become more and more important. The need for a precise model becomes especially important at medium and large signal levels or when driving the dynamic loudspeaker below its resonance frequency, as it is for example at speakers for mobile phones the case. In the small-signal domain, a linear transfer function describes the input-output relationship completely. But for high amplitudes, dynamic loudspeakers behave differently, which indicates nonlinearities. Those nonlinearities mostly depend on the displacement of the voice coil. In order to extend the validity of the model into the nonlinear domain (not part of this project), accurate prediction of the voice coil displacement is required. [1–3]

The presented master project is based on the bachelor thesis *Elektroakustische Modellbildung und Optimierung von Lautsprechersystemen* by Florian Loacker-Schöch [4] and refines the electroacoustic model of a dynamic loudspeaker for a more accurate prediction of the performance.

The standard equivalent circuit diagram for modelling the electrical and mechanical part of a dynamic loudspeaker can be seen in figure 1.1. It is based on a well-known circuit [4, p. 18].

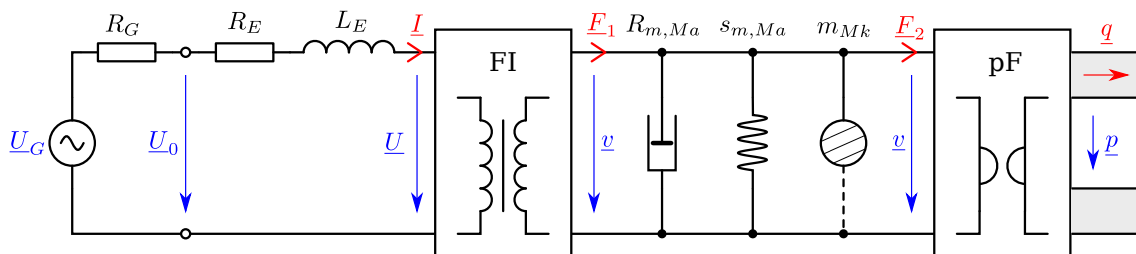


Figure 1.1: Basic equivalent circuit diagram for a dynamic loudspeaker

In the following chapters, improvements in the models for the voice coil impedance and diaphragm suspension will be made. This means that the voice coil inductance  $L_E$  will be replaced with a frequency-dependent impedance  $\underline{Z}_{L_E}(\omega)$  and the mechanical stiffness  $s_{m, Ma}$  will be replaced with a frequency-dependent impedance  $\underline{Z}_C(\omega)$ .

# 2

## Voice coil impedance modelling

In order to describe the performance of a dynamic loudspeaker more accurately, one must consider the voice coil impedance at higher frequencies. Since the voice coil does not operate in free air (there are pole tips, the magnet, the former, copper rings, etc.), the impedance can only be roughly modelled using a resistor  $R_E$  and an inductor  $L_E$ . Eddy currents usually decrease the inductance of the coil and increase losses at higher frequencies.

In this chapter, a total of 5 models for the voice coil impedance are presented, each having a frequency-dependent voice coil impedance  $\underline{Z}_{L_E}(\omega) = R_{L_E}(\omega) + j\omega L_E(\omega)$ . All model parameters may have any real value greater than zero. The associated equivalent circuit diagram can be seen in figure 2.1.

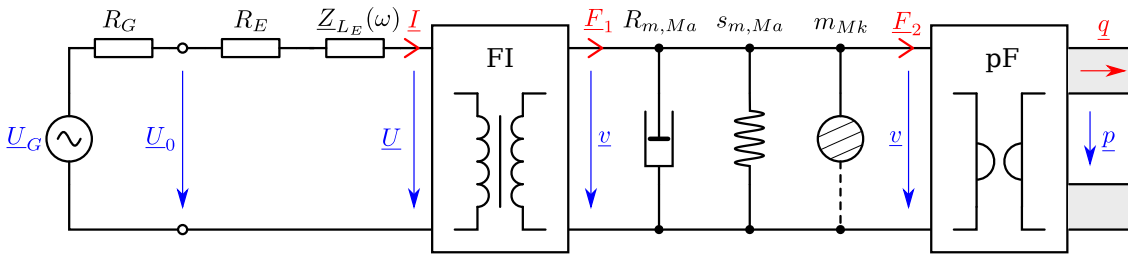


Figure 2.1: Equivalent circuit diagram for a dynamic loudspeaker when using advanced models for the voice coil impedance  $\underline{Z}_{L_E}(\omega)$

### 2.1 L2R

The L2R model [5–7] is one of the most commonly used models, as it is quite simple and can be realized as an electrical circuit as shown in figure 2.2 on the facing page. It has been applied in most audio measurement systems. This model has three parameters ( $L_E$ ,  $L_2$  and  $R_2$ ) and the associated voice coil impedance function is given by

$$\underline{Z}_{L_E}(\omega) = j\omega L_E + \frac{R_2 \cdot j\omega L_2}{R_2 + j\omega L_2} = \quad (2.1)$$

$$= \underbrace{\frac{\omega^2 L_2^2}{1 + \left(\omega \frac{L_2}{R_2}\right)^2}}_{R_{L_E}(\omega)} + j\omega \underbrace{\left( L_E + \frac{L_2}{1 + \left(\omega \frac{L_2}{R_2}\right)^2} \right)}_{L_E(\omega)}. \quad (2.2)$$

The resistance  $R_{L_E}(\omega)$  and inductance  $L_E(\omega)$  are visualized in figure 2.3 on the next page. It can be seen that the resistance increases from 0 to  $R_2$  and the inductance decreases from  $L_E + L_2$

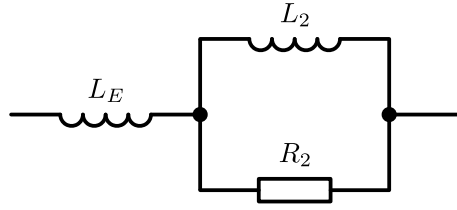


Figure 2.2: Circuit diagram for the voice coil impedance  $\underline{Z}_{L_E}(\omega)$  using the L2R model

to  $L_E$  with increasing frequency.

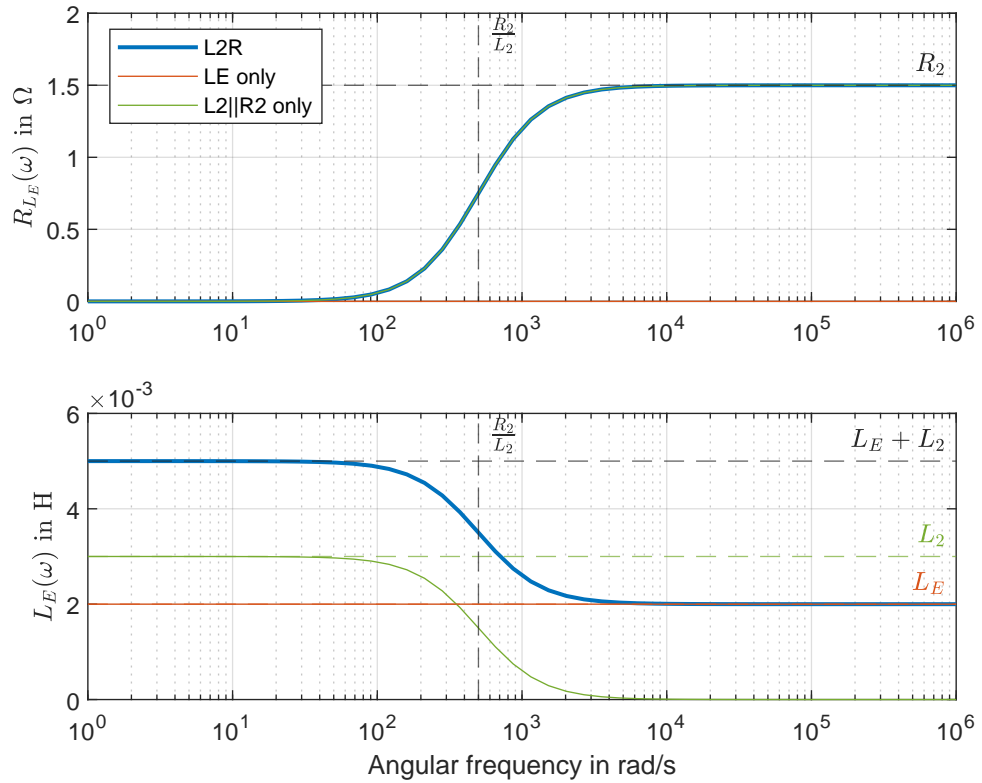


Figure 2.3: Resistance  $R_{L_E}(\omega)$  and inductance  $L_E(\omega)$  for the L2R model ( $L_E = 2$  mH,  $L_2 = 3$  mH,  $R_2 = 1.5$   $\Omega$ )

## 2.2 L3R

The L3R model [5, 6] extends the L2R model in section 2.1 on the facing page with another inductor and resistor in parallel, providing better simulation results for the lossy inductor. The circuit diagram can be seen in figure 2.4 on the next page. This model has five parameters ( $L_E$ ,  $L_2$ ,  $R_2$ ,  $L_3$  and  $R_3$ ) and the associated voice coil impedance function is given by

$$\underline{Z}_{L_E}(\omega) = j\omega L_E + \frac{R_2 \cdot j\omega L_2}{R_2 + j\omega L_2} + \frac{R_3 \cdot j\omega L_3}{R_3 + j\omega L_3} = \quad (2.3)$$

$$= \underbrace{\frac{\omega^2 \frac{L_2^2}{R_2}}{1 + \left(\omega \frac{L_2}{R_2}\right)^2} + \frac{\omega^2 \frac{L_3^2}{R_3}}{1 + \left(\omega \frac{L_3}{R_3}\right)^2}}_{R_{L_E}(\omega)} + j\omega \underbrace{\left( L_E + \frac{L_2}{1 + \left(\omega \frac{L_2}{R_2}\right)^2} + \frac{L_3}{1 + \left(\omega \frac{L_3}{R_3}\right)^2} \right)}_{L_E(\omega)}. \quad (2.4)$$

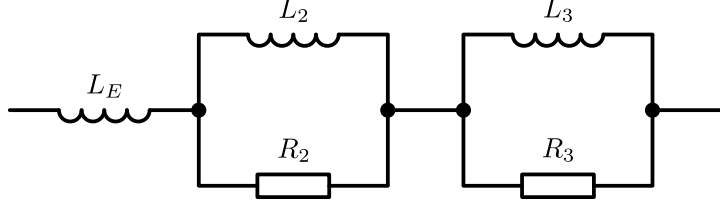


Figure 2.4: Circuit diagram for the voice coil impedance  $Z_{L_E}(\omega)$  using the L3R model

The resistance  $R_{L_E}(\omega)$  and inductance  $L_E(\omega)$  are visualized in figure 2.5. It can be seen that the resistance increases from 0 to  $R_2 + R_3$  and the inductance decreases from  $L_E + L_2 + L_3$  to  $L_E$  with increasing frequency. There may also be a plateau between  $\frac{R_2}{L_2}$  and  $\frac{R_3}{L_3}$  depending on the distance of those two frequencies.

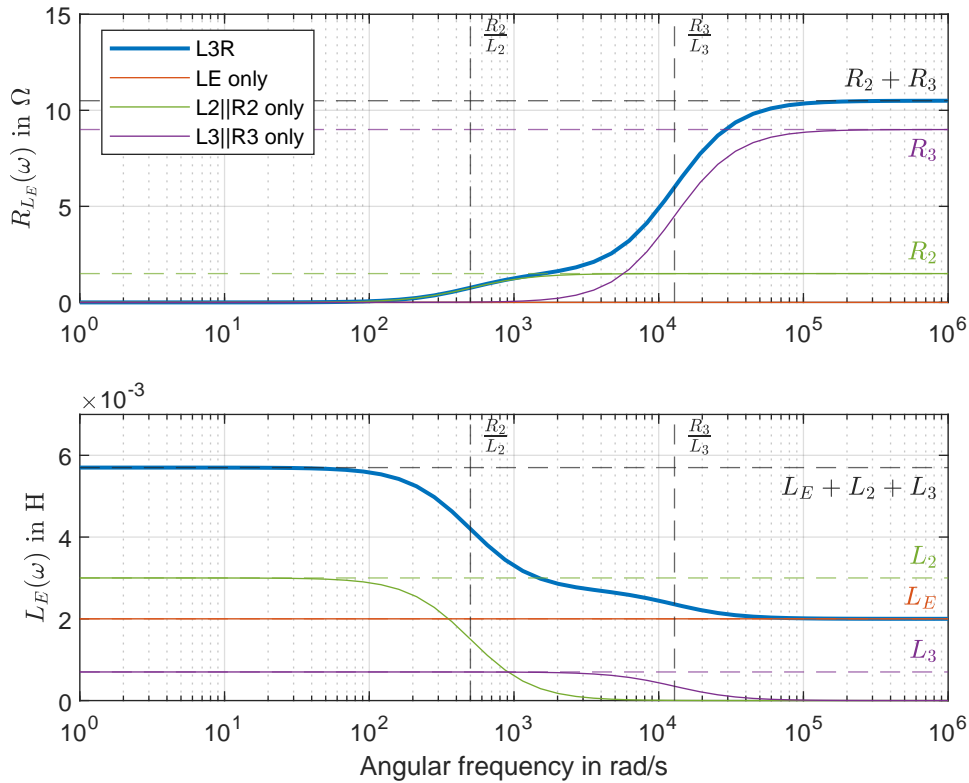


Figure 2.5: Resistance  $R_{L_E}(\omega)$  and inductance  $L_E(\omega)$  for the L3R model ( $L_E = 2$  mH,  $L_2 = 3$  mH,  $R_2 = 1.5 \Omega$ ,  $L_3 = 0.7$  mH,  $R_3 = 9 \Omega$ )

## 2.3 L2RK

The L2RK model [5, 6] extends the L2R model in section 2.1 on page 2 by adding a semi inductance  $K_2$  in parallel to  $R_2$  and  $L_2$ . The circuit diagram can be seen in figure 2.6. This model has four parameters ( $L_E$ ,  $L_2$ ,  $R_2$  and  $K_2$ ) and the associated voice coil impedance function is given by

$$\underline{Z}_{L_E}(\omega) = j\omega L_E + \frac{1}{\frac{1}{R_2} + \frac{1}{j\omega L_2} + \frac{1}{\sqrt{j\omega} K_2}} = \quad (2.5)$$

$$= \frac{\omega R_2 L_2^2 K_2 (\omega K_2 + \sqrt{\frac{\omega}{2}} R_2)}{\underbrace{R_2^2 K_2^2 + \omega R_2^2 L_2^2 + \omega^2 L_2^2 K_2^2 + \sqrt{2\omega} R_2 L_2 K_2 (R_2 + \omega L_2)}_{R_{L_E}(\omega)}} \quad (2.6)$$

$$+ j\omega \left( L_E + \underbrace{\frac{R_2^2 L_2 K_2 (K_2 + \sqrt{\frac{\omega}{2}} L_2)}{R_2^2 K_2^2 + \omega R_2^2 L_2^2 + \omega^2 L_2^2 K_2^2 + \sqrt{2\omega} R_2 L_2 K_2 (R_2 + \omega L_2)}}_{L_E(\omega)} \right). \quad (2.7)$$

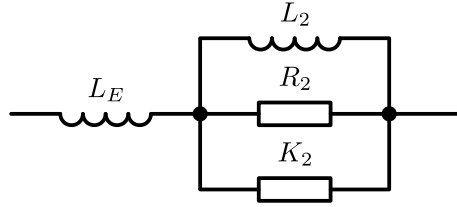


Figure 2.6: Standard circuit diagram for the voice coil impedance  $\underline{Z}_{L_E}(\omega)$  using the L2RK model

The resistance  $R_{L_E}(\omega)$  and inductance  $L_E(\omega)$  are visualized in figure 2.7 on the next page. It can be seen that the resistance increases from 0 to  $R_2$  and the inductance decreases from  $L_E + L_2$  to  $L_E$  with increasing frequency. However, in contrary to the L2R model, the slope decreases with a decreasing semi-inductance  $K_2$ .

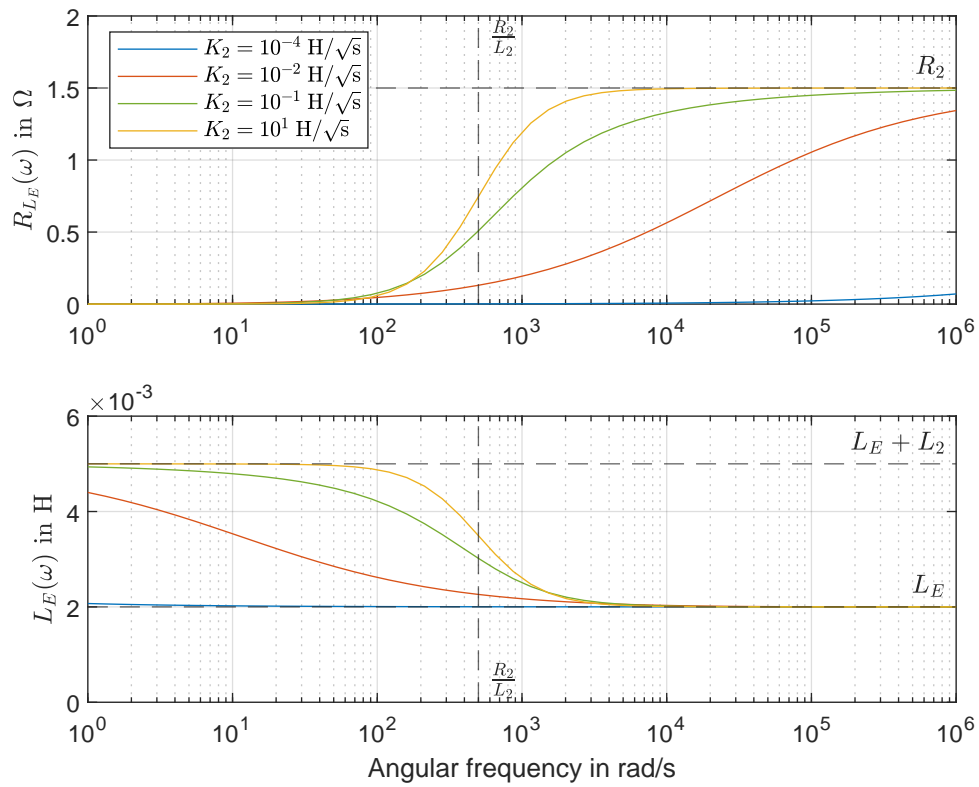


Figure 2.7: Resistance  $R_{L_E}(\omega)$  and inductance  $L_E(\omega)$  for the  $L_2RK$  model ( $L_E = 2 \text{ mH}$ ,  $L_2 = 3 \text{ mH}$ ,  $R_2 = 1.5 \Omega$ )

## 2.4 Leach

M. Leach [7,8] proposed a weighted power function of the complex frequency as an approximation for the voice coil impedance. It has only two parameters ( $K$ ,  $n$ ) and usually gives a very good fit over a wide frequency range. The associated voice coil impedance function is given by

$$\underline{Z}_{LE}(\omega) = K \cdot \left( j \frac{\omega}{\omega_0} \right)^n \quad (2.8)$$

$$= \underbrace{K \left( \frac{\omega}{\omega_0} \right)^n \cos \left( n \frac{\pi}{2} \right)}_{R_{LE}(\omega)} + j \omega \underbrace{K \frac{\omega^{n-1}}{\omega_0^n} \sin \left( n \frac{\pi}{2} \right)}_{L_E(\omega)} \quad (2.9)$$

with

$$\omega_0 = 1 \frac{\text{rad}}{\text{s}}. \quad (2.10)$$

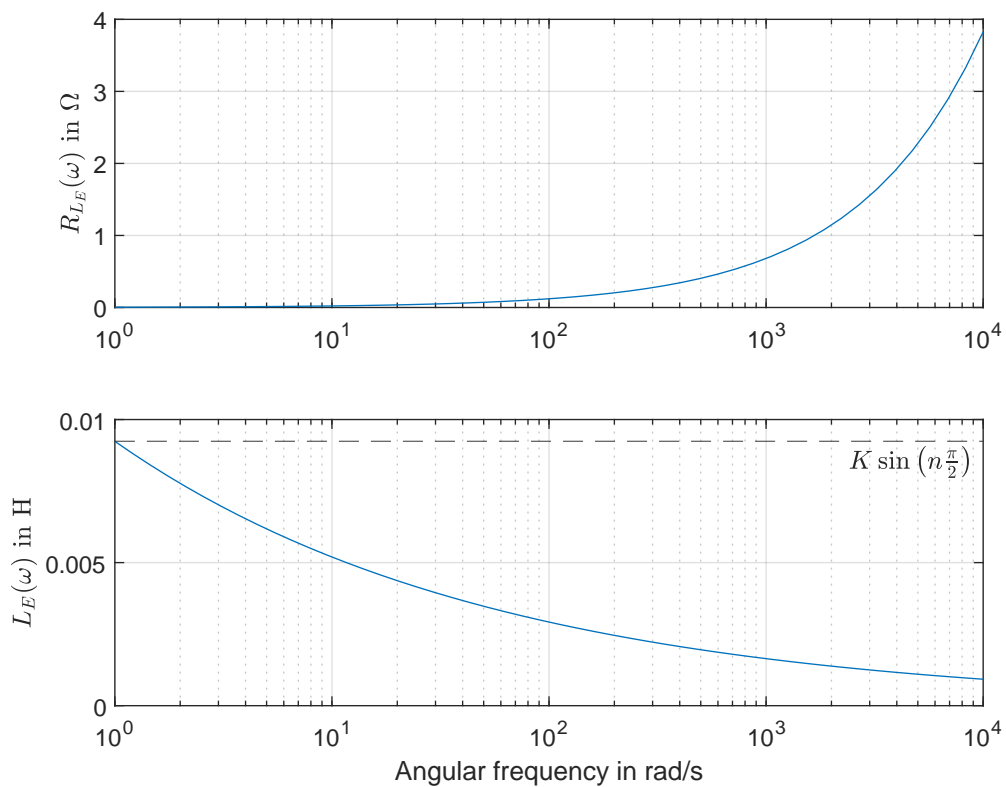


Figure 2.8: Resistance  $R_{LE}(\omega)$  and inductance  $L_E(\omega)$  for the Leach model ( $K = 0.01 \Omega$ ,  $n = 0.75$ )

## 2.5 Wright

J. Wright [7,9] proposed a model using separated weighted power functions in  $\omega$  for the real and imaginary part of the voice coil impedance. It usually gives a better fit than the L2R model in section 2.1 on page 2 and the model by Leach in section 2.4 on the previous page. It has four parameters ( $K_r$ ,  $E_r$ ,  $K_x$ ,  $E_x$ ) and the associated voice coil impedance function is given by

$$\underline{Z}_{LE}(\omega) = \underbrace{K_r \left( \frac{\omega}{\omega_0} \right)^{E_r}}_{R_{LE}(\omega)} + j\omega \underbrace{K_x \frac{\omega^{E_x-1}}{\omega_0^{E_x}}}_{L_E(\omega)} \quad (2.11)$$

with

$$\omega_0 = 1 \frac{\text{rad}}{\text{s}}. \quad (2.12)$$

The Klippel system [10] uses the symbols  $K_{rm}$ ,  $E_{rm}$ ,  $K_{xm}$  and  $E_{xm}$  respectively.

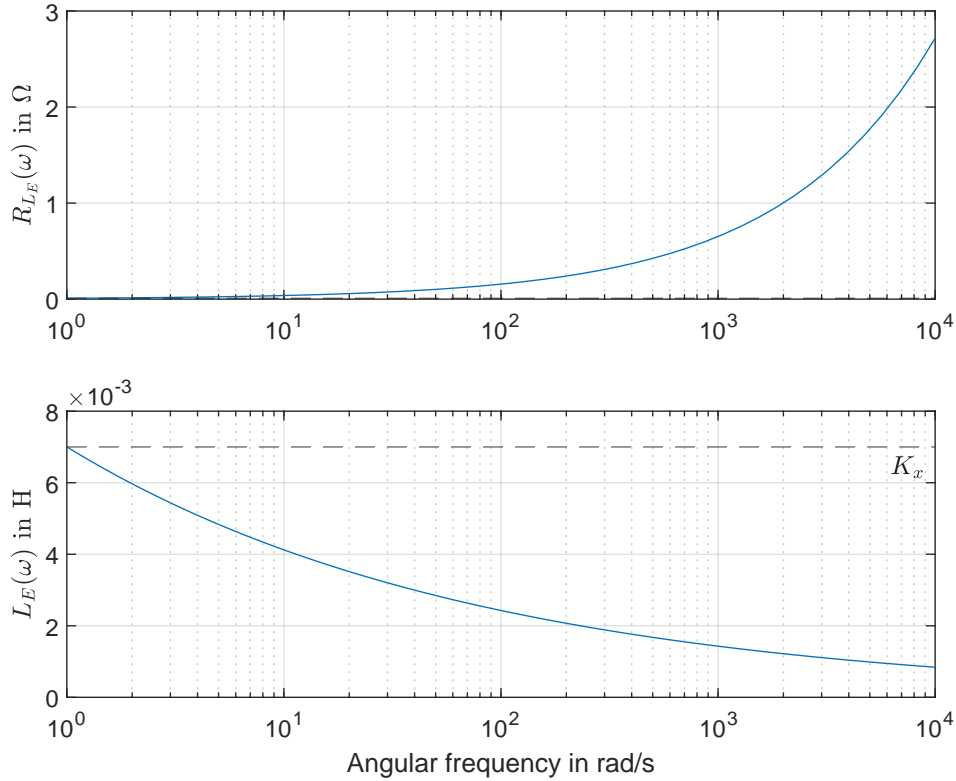


Figure 2.9: Resistance  $R_{LE}(\omega)$  and inductance  $L_E(\omega)$  for the Wright model ( $K_r = 0.009 \Omega$ ,  $E_r = 0.62$ ,  $K_x = 0.007 \Omega$ ,  $E_x = 0.77$ )

# 3

## Suspension creep modelling

The simple dynamic loudspeaker model (mass-spring-damper system) does not account for the viscoelastic creep at low frequencies observed in measurements. In real world dynamic loudspeakers the voice coil displacement continues to increase below the resonance frequency.

In all subsequent models the viscoelastic creep of the suspension is modelled by a frequency-dependent compliance  $\underline{C}(\omega)$  and the consequent impedance

$$\underline{Z}_C(\omega) = \frac{1}{j\omega\underline{C}(\omega)}. \quad (3.1)$$

All model parameters may have any real value greater than zero. The equivalent circuit diagram can be seen in figure 3.1.

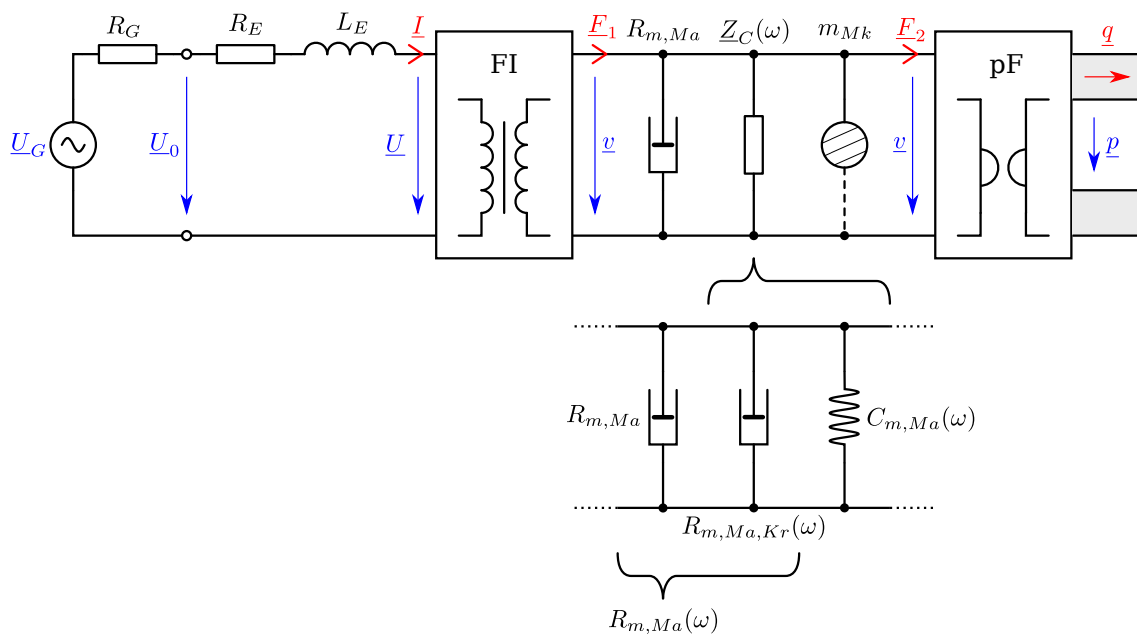


Figure 3.1: Equivalent circuit diagram for a dynamic loudspeaker when taking into account suspension creep

For models that provide a complex-valued compliance  $\underline{C}(\omega)$ , interpreting it as an ideal spring is not appropriate anymore [11, p. 2]. Its impedance  $\underline{Z}_C(\omega)$  can, however, be split up into a spring with the compliance  $C_{m,Ma}(\omega)$  and a dashpot with the resistance  $R_{m,Ma,Kr}(\omega)$  using

$$C_{m,Ma}(\omega) = \frac{|\underline{C}(\omega)|^2}{\text{Re}\{\underline{C}(\omega)\}} \quad (3.2)$$

and

$$R_{m,Ma,Kr}(\omega) = -\frac{\text{Im}\{\underline{C}(\omega)\}}{\omega |\underline{C}(\omega)|^2}. \quad (3.3)$$

*Proof.*

$$\begin{aligned} \underline{Z}_C(\omega) &= \frac{1}{j\omega \underline{C}(\omega)} = \frac{1}{j\omega (\text{Re}\{\underline{C}(\omega)\} + j\text{Im}\{\underline{C}(\omega)\})} = \\ &= \frac{1}{-\omega \text{Im}\{\underline{C}(\omega)\} + j\omega \text{Re}\{\underline{C}(\omega)\}} \cdot \frac{-\omega \text{Im}\{\underline{C}(\omega)\} - j\omega \text{Re}\{\underline{C}(\omega)\}}{-\omega \text{Im}\{\underline{C}(\omega)\} - j\omega \text{Re}\{\underline{C}(\omega)\}} = \\ &= \frac{-\omega \text{Im}\{\underline{C}(\omega)\} - j\omega \text{Re}\{\underline{C}(\omega)\}}{\omega^2 \text{Im}\{\underline{C}(\omega)\}^2 + \omega^2 \text{Re}\{\underline{C}(\omega)\}^2} = \frac{-\text{Im}\{\underline{C}(\omega)\} - j\text{Re}\{\underline{C}(\omega)\}}{\omega |\underline{C}(\omega)|^2} = \\ &= -\frac{\text{Im}\{\underline{C}(\omega)\}}{\omega |\underline{C}(\omega)|^2} + \frac{\text{Re}\{\underline{C}(\omega)\}}{j\omega |\underline{C}(\omega)|^2} \stackrel{!}{=} R_{m,Ma,Kr}(\omega) + \frac{1}{j\omega C_{m,Ma}(\omega)} \quad \square \end{aligned} \quad (3.4)$$

The resistance  $R_{m,Ma}(\omega)$  is then the sum of the mechanical resistance of the suspension and the “resistance” part of the suspension compliance.

$$R_{m,Ma}(\omega) = R_{m,Ma} + R_{m,Ma,Kr}(\omega). \quad (3.5)$$

For models that provide a real-valued compliance  $C(\omega) = C_{m,Ma}(\omega)$  follows that  $R_{m,Ma}(\omega) = R_{m,Ma}$ .

### 3.1 Standard linear solid model

A common mechanical model of viscoelasticity is the so-called Standard Linear Solid (SLS) model [2,12]. It consists of two systems in series. The first contains only a spring. The second contains a spring and a dashpot in parallel. This representation is called the Kelvin representation and can be seen in figure 3.2. The model has three parameters ( $C_0$ ,  $C_1$ ,  $\eta_1$ ) and its compliance is given by

$$\underline{C}(\omega) = C_0 + \frac{1}{\frac{1}{C_1} + j\omega\eta_1} = \quad (3.6)$$

$$= C_0 + \frac{C_1}{1 + (\omega\eta_1 C_1)^2} - j \frac{\omega\eta_1 C_1^2}{1 + (\omega\eta_1 C_1)^2}. \quad (3.7)$$

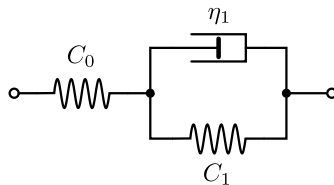


Figure 3.2: Kelvin representation of the Standard Linear Solid model

*Proof.* Equation 3.6 on the facing page can be derived by first calculating  $\underline{Z}_C(\omega)$  of the system in figure 3.2 on the preceding page and then expressing  $\underline{C}(\omega)$  from equation 3.1 on page 9.

$$\underline{Z}_C(\omega) = \frac{1}{\frac{1}{\underline{Z}_{C_0}} + \frac{1}{\underline{Z}_{C_1} + \underline{Z}_{\eta_1}}} = \frac{1}{j\omega C_0 + \frac{1}{\frac{1}{j\omega C_1} + \eta_1}} \quad (3.8)$$

$$\underline{C}(\omega) = \frac{1}{j\omega \underline{Z}_C(\omega)} = \frac{1}{j\omega} \left( j\omega C_0 + \frac{1}{\frac{1}{j\omega C_1} + \eta_1} \right) = C_0 + \frac{1}{\frac{1}{C_1} + j\omega \eta_1} \quad (3.9)$$

□

The real and imaginary parts are visualized in figure 3.3 respectively. Computational results for  $C_{m,Ma}(\omega)$  and  $R_{m,Ma,Kr}(\omega)$  using the equations 3.2 on page 9 and 3.3 on the preceding page are depicted in figure 3.4 on the following page. It can be seen that the real part of the compliance  $\underline{C}(\omega)$  and the compliance  $C_{m,Ma}(\omega)$  changes with increasing frequency from  $C_0 + C_1$  to  $C_0$ , while the resistance  $R_{m,Ma,Kr}(\omega)$  decreases to zero with increasing frequency.

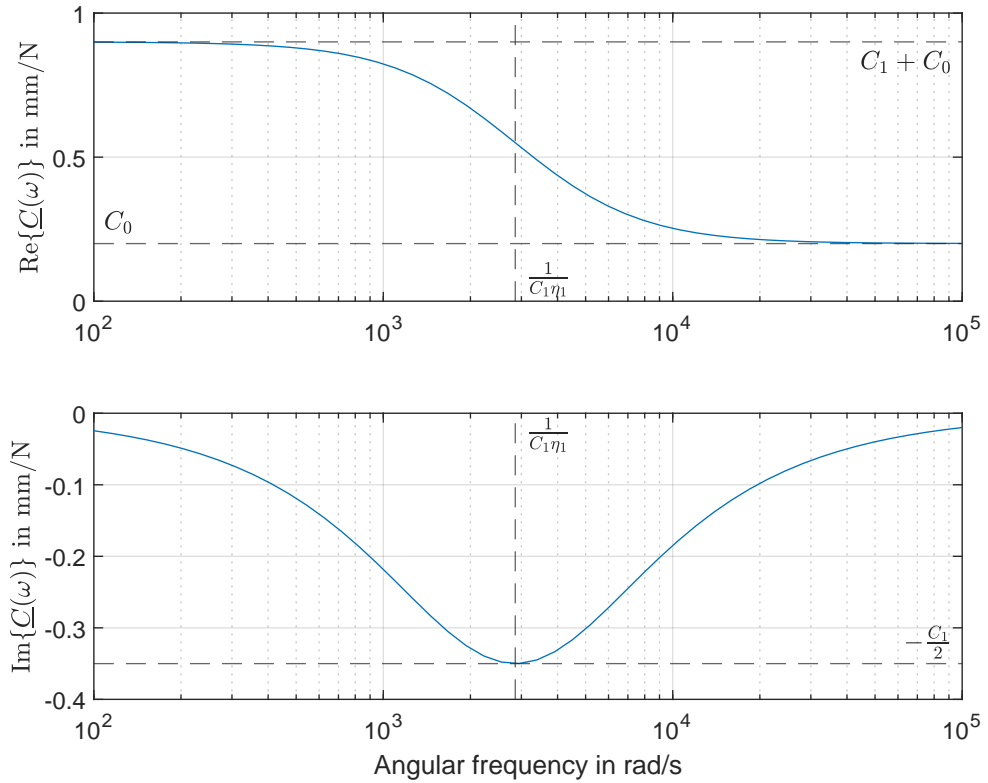


Figure 3.3: Real and imaginary parts of the compliance  $\underline{C}(\omega)$  for the SLS model ( $C_0 = 0.2 \frac{\text{m}}{\text{N}}$ ,  $C_1 = 0.7 \frac{\text{m}}{\text{N}}$ ,  $\eta_1 = 5 \times 10^{-4} \frac{\text{Ns}}{\text{m}}$ )

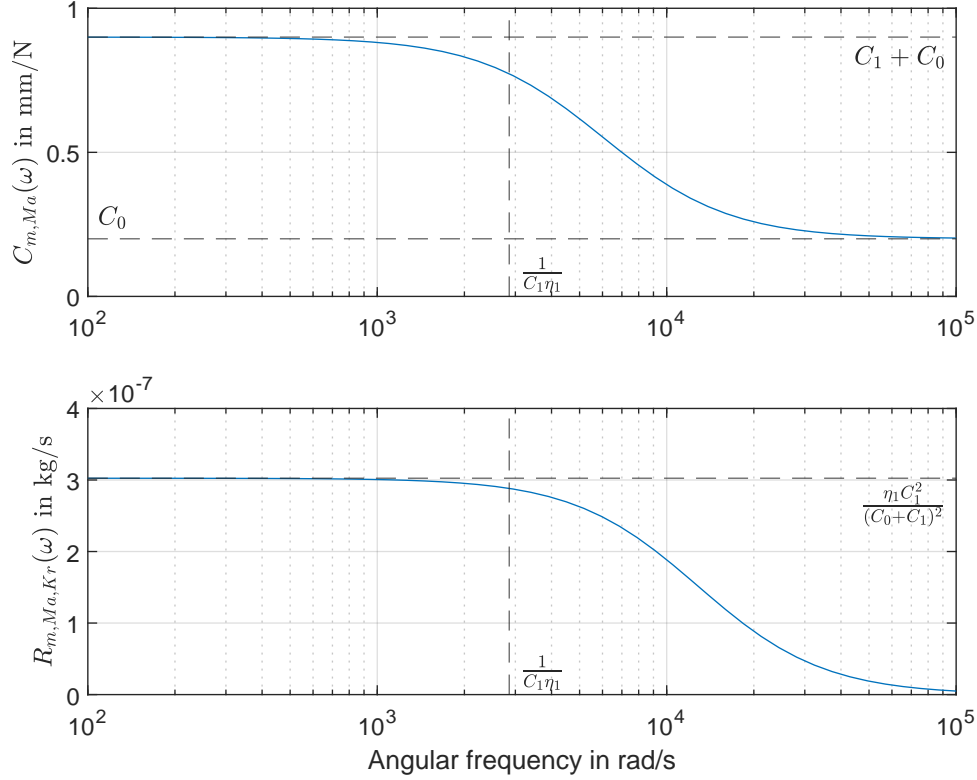


Figure 3.4: Compliance  $C_{m, Ma}(\omega)$  and resistance  $R_{m, Ma, Kr}(\omega)$  for the SLS model ( $C_0 = 0.2 \frac{\text{m}}{\text{N}}$ ,  $C_1 = 0.7 \frac{\text{m}}{\text{N}}$ ,  $\eta_1 = 5 \times 10^{-4} \frac{\text{Ns}}{\text{m}}$ )

## 3.2 Complex logarithmic model by Knudsen

Measurements have shown that when using a linear displacement magnitude scale and logarithmic frequency scale, the magnitude decreases very close to linear. This observation provided the idea of the logarithmic two-parameter creep model ( $C_0, \lambda$ ) by Knudsen [12, p. 2-3]. The compliance is given by

$$\underline{C}(\omega) = C_0 \left[ 1 - \lambda \log \left( j \frac{\omega}{\omega_0} \right) \right] \quad (3.10)$$

$$= C_0 \left[ 1 - \lambda \log \left( \frac{\omega}{\omega_0} \right) \right] - j C_0 \lambda \frac{\pi}{2 \ln(10)} \quad (3.11)$$

with

$$\omega_0 = 1 \frac{\text{rad}}{\text{s}}. \quad (3.12)$$

The real and imaginary parts are visualized in figure 3.5 on the next page respectively. Computational results for  $C_{m, Ma}(\omega)$  and  $R_{m, Ma, Kr}(\omega)$  using the equations 3.2 on page 9 and 3.3 on page 10 are depicted in figure 3.6 on page 14. It can be seen that the real part of the compliance  $\underline{C}(\omega)$  decreases steadily with increasing frequency, which causes it to become negative above the cutoff-frequency  $\omega_c = 10^{\frac{1}{\lambda}} \omega_0$ . A model which solves this problem is described in section 3.4 on page 16.

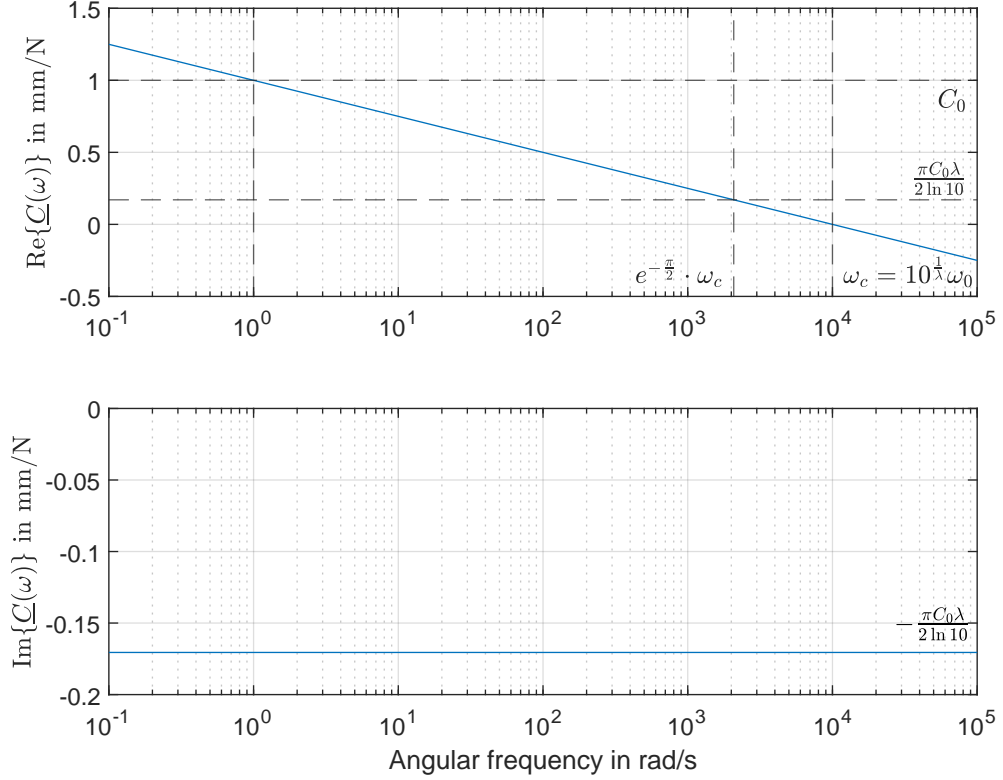


Figure 3.5: Real and imaginary parts of the compliance  $\underline{C}(\omega)$  for the complex logarithmic model by Knudsen ( $C_0 = 1 \frac{\text{m}}{\text{N}}$ ,  $\lambda = 0.25$ )

When replacing  $C_0$  and  $\lambda$  in equation 3.10 on the facing page using

$$C_0 = \tilde{C}_0 \left( 1 + \tilde{\lambda} \log \left( \frac{\omega_{uS}}{\omega_0} \right) \right) \quad (3.13)$$

and

$$\lambda = \frac{\tilde{\lambda}}{1 + \tilde{\lambda} \log \left( \frac{\omega_{uS}}{\omega_0} \right)} \quad (3.14)$$

the notation that is used by the Klippel system [11, p. 3] with a different set of parameters ( $\tilde{C}_0$  and  $\tilde{\lambda}$ ) can be derived.  $\omega_{uS}$  represents the angular resonance frequency of the dynamic loudspeaker in an infinite baffle.

*Proof.*

$$\begin{aligned} \underline{C}(\omega) &= \tilde{C}_0 \left( 1 + \tilde{\lambda} \log \left( \frac{\omega_{uS}}{\omega_0} \right) \right) \left[ 1 - \frac{\tilde{\lambda}}{1 + \tilde{\lambda} \log \left( \frac{\omega_{uS}}{\omega_0} \right)} \log \left( j \frac{\omega}{\omega_0} \right) \right] = \\ &= \tilde{C}_0 \left[ 1 + \tilde{\lambda} \log \left( \frac{\omega_{uS}}{\omega_0} \right) - \frac{1 + \tilde{\lambda} \log \left( \frac{\omega_{uS}}{\omega_0} \right)}{1 + \tilde{\lambda} \log \left( \frac{\omega_{uS}}{\omega_0} \right)} \tilde{\lambda} \log \left( j \frac{\omega}{\omega_0} \right) \right] = \end{aligned} \quad (3.15)$$

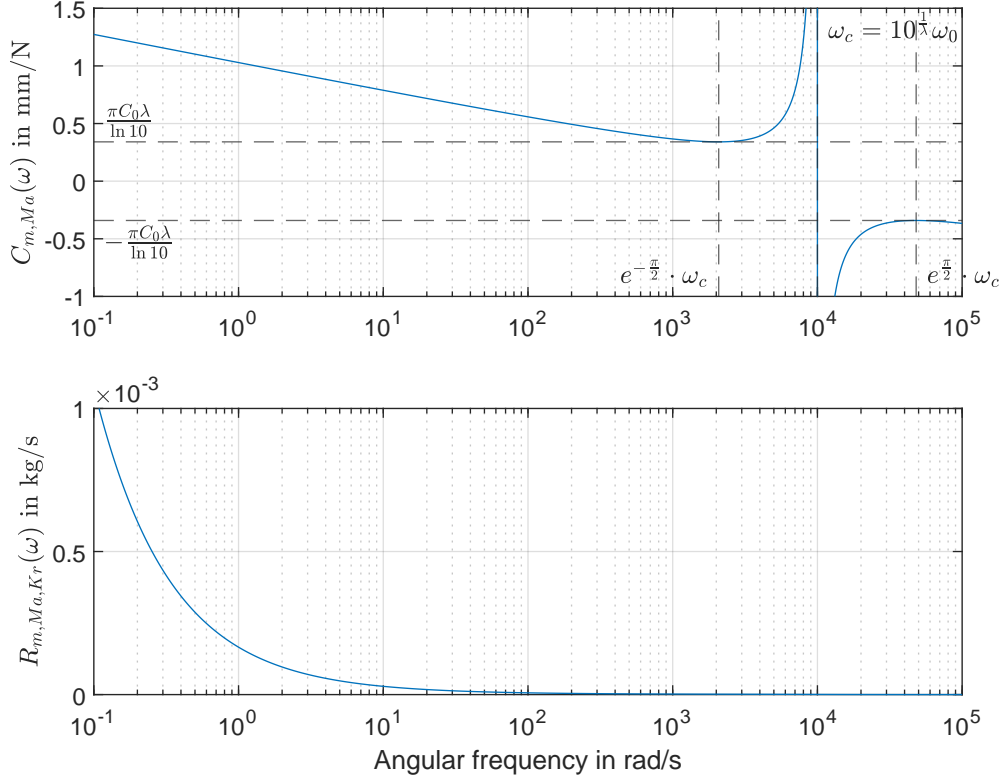


Figure 3.6: Compliance  $C_{m, Ma}(\omega)$  and resistance  $R_{m, Ma, Kr}(\omega)$  for the complex logarithmic model by Knudsen ( $C_0 = 1 \frac{\text{m}}{\text{N}}$ ,  $\lambda = 0.25$ )

$$\begin{aligned}
 &= \tilde{C}_0 \left[ 1 - \tilde{\lambda} \left( -\log\left(\frac{\omega_{uS}}{\omega_0}\right) + \log\left(j \frac{\omega}{\omega_0}\right) \right) \right] = \\
 &= \tilde{C}_0 \left[ 1 - \tilde{\lambda} \log\left(j \frac{\omega}{\omega_{uS}}\right) \right]
 \end{aligned}$$

□

### 3.3 Simplified logarithmic model by Knudsen

The complex logarithmic model as described in section 3.2 on page 12 can be approximated using

$$C(\omega) = C_0 \left[ 1 - \lambda \log\left(\frac{\omega}{\omega_0}\right) \right] \quad (3.16)$$

with

$$\omega_0 = 1 \frac{\text{rad}}{\text{s}}, \quad (3.17)$$

i.e. the imaginary part is neglected. As visualized in figure 3.5 on the preceding page, this is because

$$|\text{Im}\{\underline{C}(\omega)\}| \ll |\text{Re}\{\underline{C}(\omega)\}| \quad (3.18)$$

for

$$\omega \ll e^{-\frac{\pi}{2}} \omega_c \approx 0.2\omega_c, \quad (3.19)$$

where  $\omega_c = 10^{\frac{1}{\lambda}} \omega_0$ .

Since the imaginary part of the compliance  $\underline{C}(\omega)$  of this model is zero, the resistance  $R_{m, Ma, Kr}(\omega) = 0$  and the compliance  $C_{m, Ma}(\omega) = C(\omega)$  is the same as the real part of the compliance of the complex logarithmic model by Knudsen in equation 3.10 on page 12 as depicted in figure 3.5 on page 13.

*Proof.* The condition 3.19 can be derived by inserting the equation 3.10 on page 12 into the inequation 3.18 on the preceding page.

$$|\text{Im}\{\underline{C}(\omega)\}| \ll |\text{Re}\{\underline{C}(\omega)\}| \quad (3.20)$$

$$C_0 \lambda |\text{Im}\left\{\log\left(j \frac{\omega}{\omega_0}\right)\right\}| \ll C_0 (1 - \lambda |\text{Re}\left\{\log\left(j \frac{\omega}{\omega_0}\right)\right\}|) \quad (3.21)$$

At this point the logarithm of a purely imaginary number

$$\log\left(j \frac{\omega}{\omega_0}\right) = \log\left(\frac{\omega}{\omega_0}\right) + j \frac{\pi}{2 \ln(10)} \quad (3.22)$$

is inserted and then the inequation is solved by  $\omega$ .

$$\frac{\pi}{2 \ln(10)} C_0 \lambda \ll C_0 (1 - \lambda \log\left(\frac{\omega}{\omega_0}\right)) \quad (3.23)$$

$$\frac{\pi}{2 \ln(10)} \lambda \ll 1 - \lambda \log\left(\frac{\omega}{\omega_0}\right) \quad (3.24)$$

$$\frac{\pi}{2 \ln(10)} + \log\left(\frac{\omega}{\omega_0}\right) \ll \frac{1}{\lambda} \quad (3.25)$$

$$10^{\frac{\pi}{2 \ln(10)}} \frac{\omega}{\omega_0} \ll 10^{\frac{1}{\lambda}} \quad (3.26)$$

$$e^{\frac{\pi}{2}} \omega \ll \omega_c \quad (3.27)$$

$$\omega \ll \underbrace{e^{-\frac{\pi}{2}}}_{\approx 0.208} \omega_c \quad (3.28)$$

□

Since the simplified logarithmic model is only an approximation of the complex logarithmic model by Knudsen, the approximation error  $e(\omega) = \frac{|\text{Im}\{\underline{C}(\omega)\}|}{|\text{Re}\{\underline{C}(\omega)\}|}$  can be limited to  $e_{max}$  up to the frequency  $\omega_{max}$  when using a  $\lambda$  smaller than  $\lambda_{max}$ , which is given as

$$\lambda_{max} = \frac{1}{\frac{0.682}{e_{max}} + \log(\omega_{max})}. \quad (3.29)$$

*Proof.*

$$\frac{|\text{Im}\{\underline{C}(\omega_{max})\}|}{|\text{Re}\{\underline{C}(\omega_{max})\}|} = e_{max} \quad (3.30)$$

$$\frac{\frac{C_0 \lambda_{max} \pi}{2 \ln(10)}}{C_0 \left[1 - \lambda_{max} \log\left(\frac{\omega_{max}}{\omega_0}\right)\right]} = e_{max} \quad (3.31)$$

$$\frac{\lambda_{max}}{1 - \lambda_{max} \log\left(\frac{\omega_{max}}{\omega_0}\right)} = \frac{2\ln(10) e_{max}}{\pi} \quad (3.32)$$

$$\frac{1}{\lambda_{max}} - \log\left(\frac{\omega_{max}}{\omega_0}\right) = \frac{\pi}{2\ln(10) e_{max}} \quad (3.33)$$

$$\frac{1}{\lambda_{max}} = \frac{\pi}{2\ln(10) e_{max}} + \log\left(\frac{\omega_{max}}{\omega_0}\right) \quad (3.34)$$

$$\lambda_{max} = \frac{1}{\frac{\pi}{2\ln(10) e_{max}} + \log\left(\frac{\omega_{max}}{\omega_0}\right)} \quad (3.35)$$

$$\lambda_{max} = \frac{1}{\frac{0.682}{e_{max}} + \log\left(\frac{\omega_{max}}{\omega_0}\right)} \quad (3.36)$$

□

Assuming a maximum frequency  $\omega_{max} = 2\pi 20 \text{ k} \frac{\text{rad}}{\text{s}}$  and a maximum error  $e_{max} = 0.01$ ,  $\lambda_{max}$  can be calculated to 0.0136. This means that within the typical audio frequency range up to 20 kHz, the simplified logarithmic model is only a good approximation for very low  $\lambda$ . This observation coincides with the statement by Klippel [10,11], that this model delivers good results for speakers with low creep effect.

### 3.4 Logarithmic models by Ritter

The creep models by Ritter et al. [2] are based on the Generalized Kelvin-Voigt model (GKV) depicted in figure 3.7, which is itself an expanded version of the the Standard Linear Solid (SLS) model depicted in figure 3.2 on page 10. Each branch in figure 3.7 has its own retardation time  $\tau_i = \eta_i C_i$ .

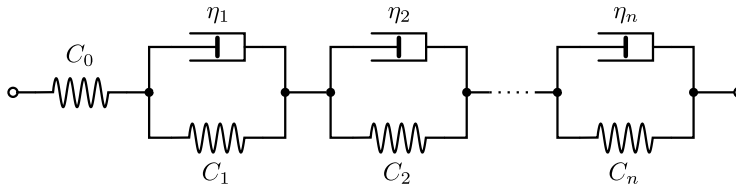


Figure 3.7: Generalized Kelvin-Voigt model with  $n$  spring-dashpot branches

In the models by Ritter et al. the GKV model is expanded such that it comprises an infinite number of branches ( $n \rightarrow \infty$ ).

The models have been created to overcome the drawbacks of the complex logarithmic model by Knudsen et al. in section 3.2 on page 12, that is the increasing compliance toward infinity as the frequency approaches zero and the negative real part of the compliance above the cutoff-frequency  $\omega_c = 10^{\frac{1}{\lambda}}$ . The three parameter model in section 3.4.1 on the facing page only addresses the drawback with the negative real part of the compliance above the cutoff-frequency  $\omega_c$ , whereas the four parameter model in section 3.4.2 on page 18 addresses both issues.

In order to understand the origin of the three and four parameter models, one have to consider

the compliance of the infinitely expanded GKV model. That is

$$\underline{C}(\omega) = \int_0^\infty \frac{L(\tau)}{\tau} \frac{1}{1 + \omega^2 \tau^2} d\tau - j \int_0^\infty \frac{L(\tau)}{\tau} \frac{\omega \tau}{1 + \omega^2 \tau^2} d\tau \quad (3.37)$$

where  $\tau$  is called the retardation time and  $L(\tau)$  the continuous retardation spectrum [2]. Ferry [13, p. 67] provided a way to calculate the retardation spectrum  $L(\tau)$  for viscoelastic polymers (in general, not just for loudspeakers) if the compliance has been measured and can be expressed as an analytic function  $\underline{C}_a(\omega)$ . For this analytic function  $\underline{C}_a(\omega)$ , Ritter et al. used the complex logarithmic model by Knudsen in equation 3.10 on page 12, as it proved to be quite accurate in predicting the suspension creep. Thus, the retardation spectrum  $L(\tau)$  then becomes [2]

$$L(\tau) = L = C_a \lambda \log(e). \quad (3.38)$$

when using

$$\underline{C}_a(\omega) = C_a [1 - \lambda \log(j\omega)]. \quad (3.39)$$

The lower limit of the integrals in equation 3.37 has to be increased to  $\tau_{min}$  because at least the first integral does not converge at  $\tau = 0$ . To compensate that, a minimum compliance  $C_0$  is added. This is why the compliance  $\underline{C}(\omega)$  does never go below the minimum compliance  $C_0$ , even above the cutoff-frequency  $\omega_c$ . Using the substitution  $\kappa = \frac{C_a}{C_0} \lambda$ , the calculation of the integrals then leads to the formula 3.40 in section 3.4.1.

Similarly, the upper limit of the integrals can be decreased to  $\tau_{max}$  in order to restrict the compliance  $\underline{C}(\omega)$  at low frequencies. Using the same substitution  $\kappa = \frac{C_a}{C_0} \lambda$ , the calculation of the integrals then leads to the formula 3.44 on the following page in section 3.4.2 on the next page.

The real and imaginary parts of the compliance  $\underline{C}(\omega)$  for the three and four parameter models are visualized in figure 3.8 on the following page respectively. Computational results for  $C_{m, Ma}(\omega)$  and  $R_{m, Ma, Kr}(\omega)$  using the equations 3.2 on page 9 and 3.3 on page 10 are depicted in figure 3.9 on page 19. In order to highlight the improvement to the complex logarithmic model by Knudsen, it has been included in those graphs as well. You can easily see that the three parameter model does only restrict the compliance at high frequencies, whereas the four parameter model does also restrict the compliance at low frequencies.

### 3.4.1 Three parameter model

The compliance for the three-parameter model ( $C_0, \kappa, \tau_{min}$ ) by Ritter et al. [2] is given by

$$\underline{C}(\omega) = C_0 \left[ 1 - \kappa \log \left( \frac{\omega \tau_{min}}{\sqrt{1 + \omega^2 \tau_{min}^2}} e^{j\phi(\omega)} \right) \right] = \quad (3.40)$$

$$= C_0 \left[ 1 - \kappa \log \left( \frac{\omega \tau_{min}}{\sqrt{1 + \omega^2 \tau_{min}^2}} \right) \right] - j \frac{C_0 \kappa}{\ln(10)} \phi(\omega) \quad (3.41)$$

with

$$\phi(\omega) = \arctan \left( \frac{1}{\omega \tau_{min}} \right). \quad (3.42)$$

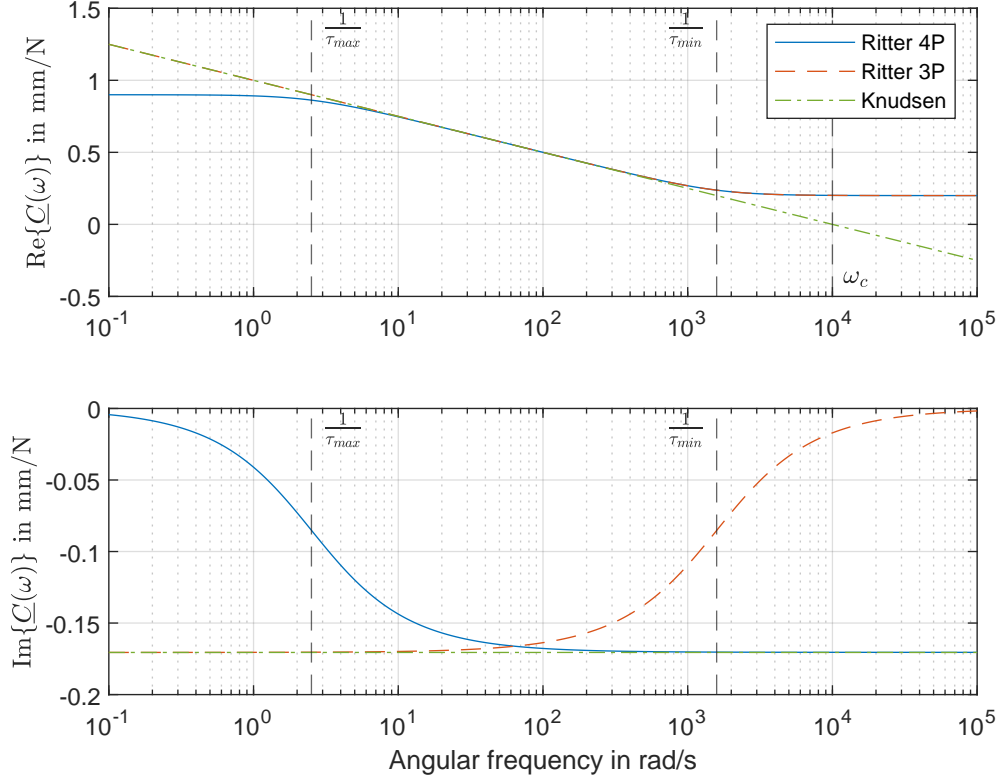


Figure 3.8: Real and imaginary parts of the compliance  $\underline{C}(\omega)$  for the logarithmic models by Ritter ( $C_0 = 0.2 \frac{\text{m}}{\text{N}}$ ,  $\kappa = 1.25$ ,  $\tau_{\min} = 6.31 \times 10^{-4} \text{ s}$ ,  $\tau_{\max} = 0.398 \text{ s}$ ) and the complex logarithmic model by Knudsen ( $C_0 = 1 \frac{\text{m}}{\text{N}}$ ,  $\lambda = 0.25$ )

When replacing  $\tau_{\min}$  using

$$\tau_{\min} = \frac{1}{\omega_{\min}} \quad (3.43)$$

the notation that is used by the Klippel system [11] with a different set of parameters ( $C_0$ ,  $\kappa$ ,  $f_{\min}$ ) can be derived.

### 3.4.2 Four parameter model

The compliance for the four-parameter model ( $C_0$ ,  $\kappa$ ,  $\tau_{\min}$ ,  $\tau_{\max}$ ) by Ritter et al. [2] is given by

$$\underline{C}(\omega) = C_0 \left[ 1 - \kappa \log \left( \sqrt{\frac{\tau_{\min}^2 + \omega^2 \tau_{\min}^2 \tau_{\max}^2}{\tau_{\max}^2 + \omega^2 \tau_{\min}^2 \tau_{\max}^2}} e^{j\phi(\omega)} \right) \right] = \quad (3.44)$$

$$= C_0 \left[ 1 - \kappa \log \left( \sqrt{\frac{\tau_{\min}^2 + \omega^2 \tau_{\min}^2 \tau_{\max}^2}{\tau_{\max}^2 + \omega^2 \tau_{\min}^2 \tau_{\max}^2}} \right) - j \frac{C_0 \kappa}{\ln(10)} \phi(\omega) \right] \quad (3.45)$$

with

$$\phi(\omega) = \arctan \left( \frac{\omega (\tau_{\max} - \tau_{\min})}{1 + \omega^2 \tau_{\max} \tau_{\min}} \right). \quad (3.46)$$

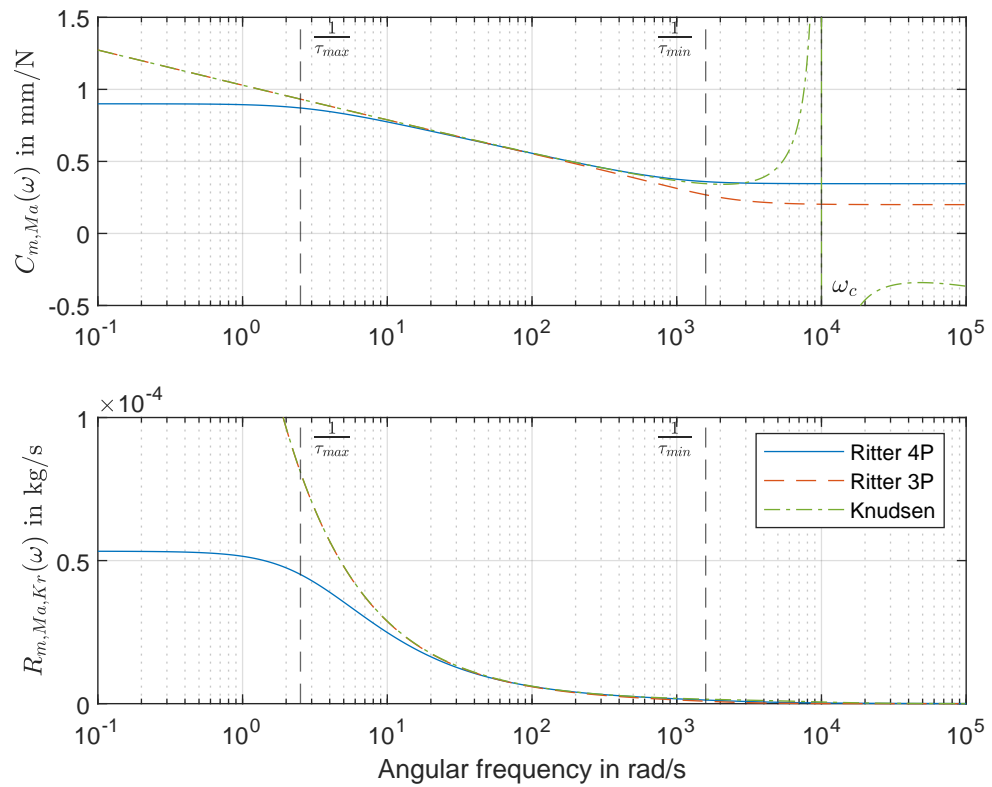


Figure 3.9: Compliance  $C_{m, Ma}(\omega)$  and resistance  $R_{m, Ma, Kr}(\omega)$  for the logarithmic models by Ritter ( $C_0 = 0.2 \frac{\text{m}}{\text{N}}$ ,  $\kappa = 1.25$ ,  $\tau_{min} = 6.31 \times 10^{-4}$  s,  $\tau_{max} = 0.398$  s) and the complex logarithmic model by Knudsen ( $C_0 = 1 \frac{\text{m}}{\text{N}}$ ,  $\lambda = 0.25$ )

## 4

## Measurements and evaluation of the advanced models

### 4.1 Overview

The setup for measuring the impedance and displacement is visualized in figure 4.1. For all measurements the *Distortion Analyzer 2* along with the software *dB-Lab Pro* by Klippel has been used, see LPM Module documentation [10] for more details on how to setup and perform the measurements. Loudspeaker parameters have been calculated either using the Klippel software or LIMP by ARTALABS [5]. Simulations have been performed using the *Speaker Analyzer 2.2* [14].

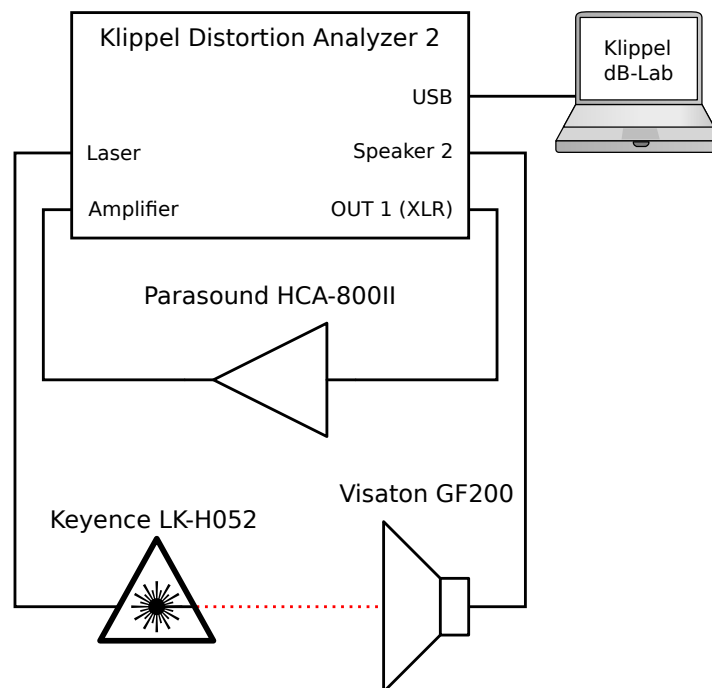


Figure 4.1: Measurement setup

A photo of the measurement setup can be seen in figure 4.2 on the next page.

All hardware and software that has been used for performing the measurements and simulations is listed in the tables 4.1 on the facing page and 4.2 on the next page.

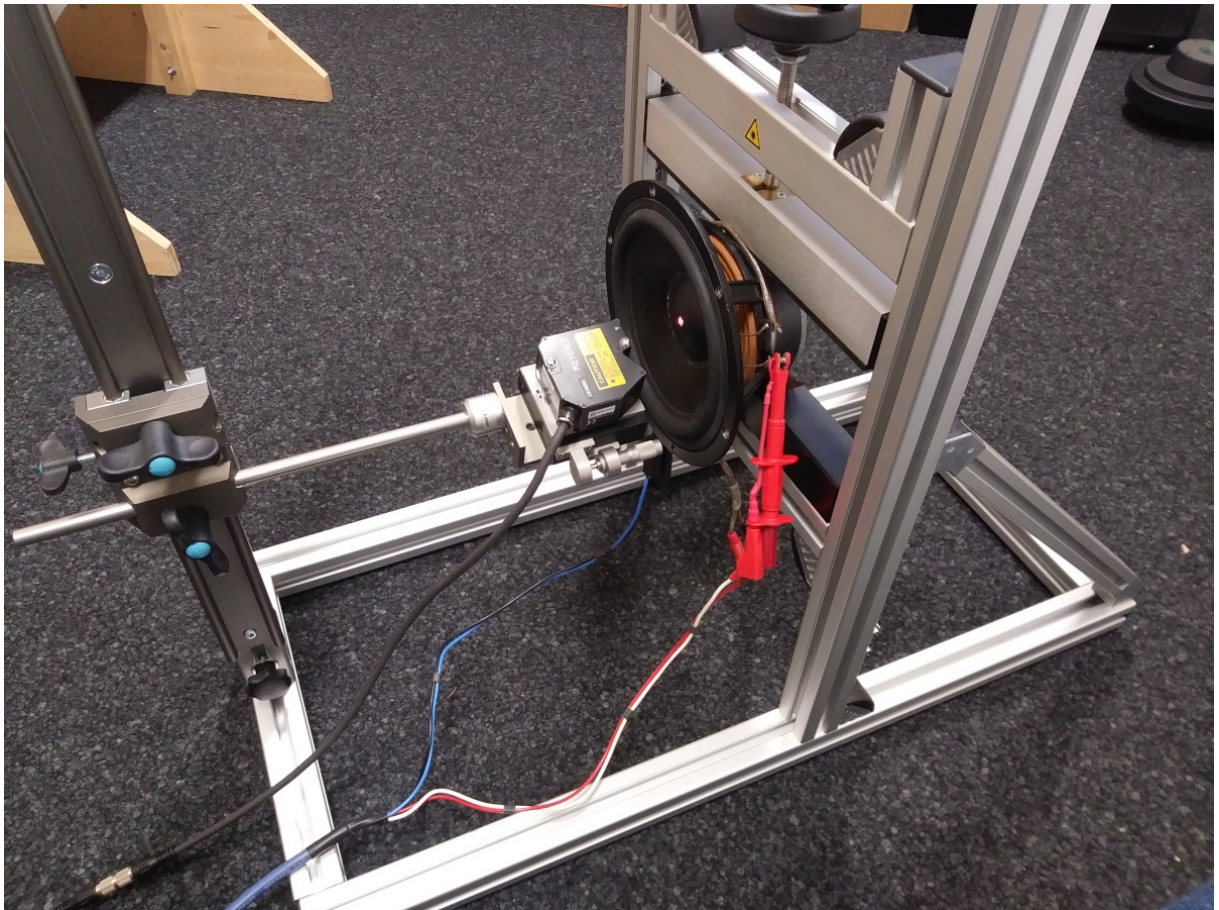


Figure 4.2: Photo of the loudspeaker in free air

Device	Brand	Model
Distortion analyzer	Klippel	DA2
Amplifier	Parasound	HCA-800II
Loudspeaker	Visaton	GF200
Mounting stand	Klippel	Pro Driver Stand
Laser	Keyence	LK-H052

Table 4.1: Used hardware

Developer	Product	Version
Klippel	dB-Lab Pro	206.350
Klippel	LPM Module	-
ARTALABS	LIMP	1.9.3
MathWorks	MATLAB	R2018b
Florian Loacker-Schöch	Speaker Analyzer	2.1
Markus Faymann	Speaker Analyzer	2.2

Table 4.2: Used software

## 4.2 Measurement and simulation procedure

The LPM Module [10] has been used to perform the impedance and displacement measurements. Since the stimulus is a combination of multiple sine signals played simultaneously, the number of frequencies per measurement is limited. In order to provide decent accuracy from 20 Hz to 18 kHz (the maximum frequency that is supported by the *Distortion Analyzer 2*), two measurements had to be made, one from 20 Hz to 2 kHz and another from 2 kHz to 18 kHz. Note the LPM Module by default includes some measurement points for lower frequencies (down to around 0.5 Hz for the impedance measurement and down to 5 Hz for the displacement measurement), which have been used as well. The data of those two measurements has been exported by selecting each impedance and displacement curve individually using the mouse, pressing Ctrl+C and then pasting the data of each curve in a separate m-file. After that *Matlab* has been used to combine the data of those two measurements (see the function `merge_klippel` in table A.2 on page 34). In total this added up to around 280 logarithmically spaced frequency points.

In order to compute the optimal parameters for the voice coil and suspension creep models that are supported by Klippel, a new object in *dB-Lab Pro* has been created using *LPM Extended Creep Modelling - AN49* template. The measurement data of the impedance and displacement has been imported into *dB-Lab Pro* and optimal parameters for various voice coil and suspension creep models have been calculated.

In order to compute the optimal parameters for the voice coil models that are supported by ARTALABS, the measurement data of the impedance is converted into a file format that is supported by *LIMP* using *Matlab* (see the function `convert_klippel_to_limp` in table A.2 on page 34) and then imported into *LIMP*. The fixed mass method has been used to calculate the optimal parameters for various voice coil models. For the static membrane mass, the previously calculated mass by Klippel has been used, i.e. 27.94 g.

After obtaining all the parameters, the impedance and displacement is computed using the function `matrix_model_calc_fA` of the *Speaker Analyzer 2.2*. In order to show the behaviour outside the measured frequency range, the frequency range of the simulation has been increased up to 20 kHz for the impedance and down to 1 Hz for the displacement. Furthermore, an increased frequency resolution has been used, so the simulated impedance and displacement curves are more smooth.

In order to provide a comparable measure for the models, the squared error  $e$  in percent between the modelled and the measured impedance (magnitude and phase) and displacement is calculated using

$$e = \frac{\sum_f [s(f) - m(f)]^2}{\sum_f m(f)^2} \cdot 100\% \quad (4.1)$$

for all subsequent measurements and simulations where  $f$  donates the measurement frequency,  $s(f)$  donates the *simulated* impedance or displacement using the *Speaker Analyzer 2.2* and  $m(f)$  donates the corresponding *measured* impedance or displacement.

In the subsequent section the simulations were named depending on what models have been used and how the parameters have been obtained. A list of all the simulation configurations is given in table 4.3 on the facing page.

Simulation name	Description
L/NoCreep/20-18k/Klippel	A simple inductor has been used for the voice coil model and no creep model has been used. The measured impedance from around 0.5 Hz to 18 kHz and measured displacement from 5 Hz to 18 kHz has been used to obtain the parameters using Klippel.
L2R/NoCreep/20-18k/Klippel	The L2R model has been used for the voice coil model and no creep model has been used. The measured impedance from around 0.5 Hz to 18 kHz and measured displacement from 5 Hz to 18 kHz has been used to obtain the parameters using Klippel.
Leach/NoCreep/20-18k/Klippel	The Leach model has been used for the voice coil model and no creep model has been used. The measured impedance from around 0.5 Hz to 18 kHz and measured displacement from 5 Hz to 18 kHz has been used to obtain the parameters using Klippel.
Wright/NoCreep/20-18k/Klippel	The Wright model has been used for the voice coil model and no creep model has been used. The measured impedance from around 0.5 Hz to 18 kHz and measured displacement from 5 Hz to 18 kHz has been used to obtain the parameters using Klippel.
L2R/NoCreep/20-18k/LIMP	The L2R model has been used for the voice coil model and no creep model has been used. The measured impedance from around 0.5 Hz to 18 kHz has been used to obtain the parameters using LIMP.
L3R/NoCreep/20-18k/LIMP	The L3R model has been used for the voice coil model and no creep model has been used. The measured impedance from around 0.5 Hz to 18 kHz has been used to obtain the parameters using LIMP.
L2RK/NoCreep/20-18k/LIMP	The L2RK model has been used for the voice coil model and no creep model has been used. The measured impedance from around 0.5 Hz to 18 kHz has been used to obtain the parameters using LIMP.
L2R/NoCreep/20-2k/Klippel	The L2R model has been used for the voice coil model and no creep model has been used. The measured impedance from around 0.5 Hz to 2 kHz and measured displacement from 5 Hz to 2 kHz has been used to obtain the parameters using Klippel.
L2R/SimpleLog/20-2k/Klippel	The L2R model has been used for the voice coil model and simple logarithmic model by Knudsen has been used for the creep model. The measured impedance from around 0.5 Hz to 2 kHz and measured displacement from 5 Hz to 2 kHz has been used to obtain the parameters using Klippel.
L2R/ComplexLog/20-2k/Klippel	The L2R model has been used for the voice coil model and complex logarithmic model by Knudsen has been used for the creep model. The measured impedance from around 0.5 Hz to 2 kHz and measured displacement from 5 Hz to 2 kHz has been used to obtain the parameters using Klippel.
L2R/Ritter3/20-2k/Klippel	The L2R model has been used for the voice coil model and three parameter logarithmic model by Ritter has been used for the creep model. The measured impedance from around 0.5 Hz to 2 kHz and measured displacement from 5 Hz to 2 kHz has been used to obtain the parameters using Klippel.

Table 4.3: Used simulation configurations

### 4.3 Measurement results in free air

The computed model parameters for all simulation configurations are listed in table 4.4 on the next page.

The measured and simulated impedance and displacement using various voice coil models for the loudspeaker in free air are visualized in the figures 4.3 to 4.5 on pages 26–28. It's squared errors are listed in the tables 4.5 to 4.6 on page 29. You can clearly see that the model which uses a simple inductor (L) yields the most deviation from the measurement. The L2R model already provides a large improvement over the simple inductor. After that the L3R and L2RK models are even more accurate, although by a much less amount. The Leach and Wright model both seem to provide the best results, with hardly any difference between them.

The measured and simulated impedance and displacement using various suspension creep models for the loudspeaker in free air are visualized in the figures 4.4 to 4.6 on pages 27–28. It's squared errors are listed in the tables 4.5 to 4.6 on page 29. Looking at the displacement, you can clearly see that the Ritter model provides the best results. The performance of the two logarithmic models by Knudsen is lower than the performance of the Ritter model. Remarkable is also that the complex logarithmic models seems to perform worse than the simplified logarithmic model. This is because the magnitude of the impedance at the resonance frequency is lower when using the complex logarithmic model.

Simulation name	Parameters
L/NoCreep/20-18k/Klippel	$R_E = 6.34 \Omega$ , $L_E = 0.39 \text{ mH}$ , $m_{Mk} = 27.567 \text{ g}$ , $R_{m,Ma} = 0.816 \frac{\text{kg}}{\text{s}}$ , $s_{m,Ma} = 0.5291 \frac{\text{N}}{\text{mm}}$ , $Bl = 9.24 \frac{\text{N}}{\text{A}}$
L2R/NoCreep/20-18k/Klippel	$R_E = 6.34 \Omega$ , $L_E = 0.39 \text{ mH}$ , $L_2 = 0.42 \text{ mH}$ , $R_2 = 16 \Omega$ , $m_{Mk} = 27.567 \text{ g}$ , $R_{m,Ma} = 0.816 \frac{\text{kg}}{\text{s}}$ , $s_{m,Ma} = 0.5291 \frac{\text{N}}{\text{mm}}$ , $Bl = 9.24 \frac{\text{N}}{\text{A}}$
Leach/NoCreep/20-18k/Klippel	$R_E = 6.34 \Omega$ , $K = 0.011126 \Omega$ , $n = 0.716$ , $m_{Mk} = 26.867 \text{ g}$ , $R_{m,Ma} = 0.794 \frac{\text{kg}}{\text{s}}$ , $s_{m,Ma} = 0.54348 \frac{\text{N}}{\text{mm}}$ , $Bl = 9.11 \frac{\text{N}}{\text{A}}$
Wright/NoCreep/20-18k/Klippel	$R_E = 6.34 \Omega$ , $K_r = 0.002443 \Omega$ , $E_r = 0.777$ , $K_x = 0.011791 \Omega$ , $E_x = 0.701$ , $m_{Mk} = 26.967 \text{ g}$ , $R_{m,Ma} = 0.8 \frac{\text{kg}}{\text{s}}$ , $s_{m,Ma} = 0.54054 \frac{\text{N}}{\text{mm}}$ , $Bl = 9.14 \frac{\text{N}}{\text{A}}$
L2R/NoCreep/20-18k/LIMP	$R_E = 6.46 \Omega$ , $L_E = 0.38454 \text{ mH}$ , $L_2 = 0.49941 \text{ mH}$ , $R_2 = 11.39 \Omega$ , $m_{Mk} = 26.177 \text{ g}$ , $R_{m,Ma} = 0.791 \frac{\text{kg}}{\text{s}}$ , $s_{m,Ma} = 0.5553 \frac{\text{N}}{\text{mm}}$ , $Bl = 8.9603 \frac{\text{N}}{\text{A}}$
L3R/NoCreep/20-18k/LIMP	$R_E = 6.46 \Omega$ , $L_E = 0.36211 \text{ mH}$ , $L_2 = 0.30684 \text{ mH}$ , $R_2 = 11.12 \Omega$ , $L_3 = 0.56941 \text{ mH}$ , $R_3 = 2.89 \Omega$ , $m_{Mk} = 26.177 \text{ g}$ , $R_{m,Ma} = 0.791 \frac{\text{kg}}{\text{s}}$ , $s_{m,Ma} = 0.5553 \frac{\text{N}}{\text{mm}}$ , $Bl = 8.9603 \frac{\text{N}}{\text{A}}$
L2RK/NoCreep/20-18k/LIMP	$R_E = 6.46 \Omega$ , $L_E = 0.25746 \text{ mH}$ , $L_2 = 1.4498 \text{ mH}$ , $R_2 = 63.3 \Omega$ , $K_2 = 0.099081 \frac{\text{H}}{\sqrt{\text{s}}}$ , $m_{Mk} = 26.177 \text{ g}$ , $R_{m,Ma} = 0.791 \frac{\text{kg}}{\text{s}}$ , $s_{m,Ma} = 0.5553 \frac{\text{N}}{\text{mm}}$ , $Bl = 8.9603 \frac{\text{N}}{\text{A}}$
L2R/NoCreep/20-2k/Klippel	$R_E = 6.34 \Omega$ , $L_E = 0.76 \text{ mH}$ , $L_2 = 0.58 \text{ mH}$ , $R_2 = 3.1 \Omega$ , $m_{Mk} = 27.667 \text{ g}$ , $R_{m,Ma} = 0.82 \frac{\text{kg}}{\text{s}}$ , $s_{m,Ma} = 0.52632 \frac{\text{N}}{\text{mm}}$ , $Bl = 9.26 \frac{\text{N}}{\text{A}}$
L2R/SimpleLog/20-2k/Klippel	$R_E = 6.34 \Omega$ , $L_E = 0.76 \text{ mH}$ , $L_2 = 0.58 \text{ mH}$ , $R_2 = 3.1 \Omega$ , $m_{Mk} = 28.067 \text{ g}$ , $R_{m,Ma} = 0.822 \frac{\text{kg}}{\text{s}}$ , $C_0 = 0.58075 \frac{\text{mm}}{\text{N}}$ , $\lambda = 0.043062$ , $Bl = 9.27 \frac{\text{N}}{\text{A}}$
L2R/ComplexLog/20-2k/Klippel	$R_E = 6.34 \Omega$ , $L_E = 0.76 \text{ mH}$ , $L_2 = 0.58 \text{ mH}$ , $R_2 = 3.1 \Omega$ , $m_{Mk} = 27.867 \text{ g}$ , $R_{m,Ma} = 0.813 \frac{\text{kg}}{\text{s}}$ , $C_0 = 0.57658 \frac{\text{mm}}{\text{N}}$ , $\lambda = 0.03817$ , $Bl = 9.25 \frac{\text{N}}{\text{A}}$
L2R/Ritter3/20-2k/Klippel	$R_E = 6.34 \Omega$ , $L_E = 0.76 \text{ mH}$ , $L_2 = 0.58 \text{ mH}$ , $R_2 = 3.1 \Omega$ , $m_{Mk} = 28.067 \text{ g}$ , $R_{m,Ma} = 0.378 \frac{\text{kg}}{\text{s}}$ , $C_0 = 0.504 \frac{\text{mm}}{\text{N}}$ , $\kappa = 0.14$ , $\tau_{min} = 3.1207 \text{ ms}$ , $Bl = 9.22 \frac{\text{N}}{\text{A}}$

Table 4.4: Computed model parameters

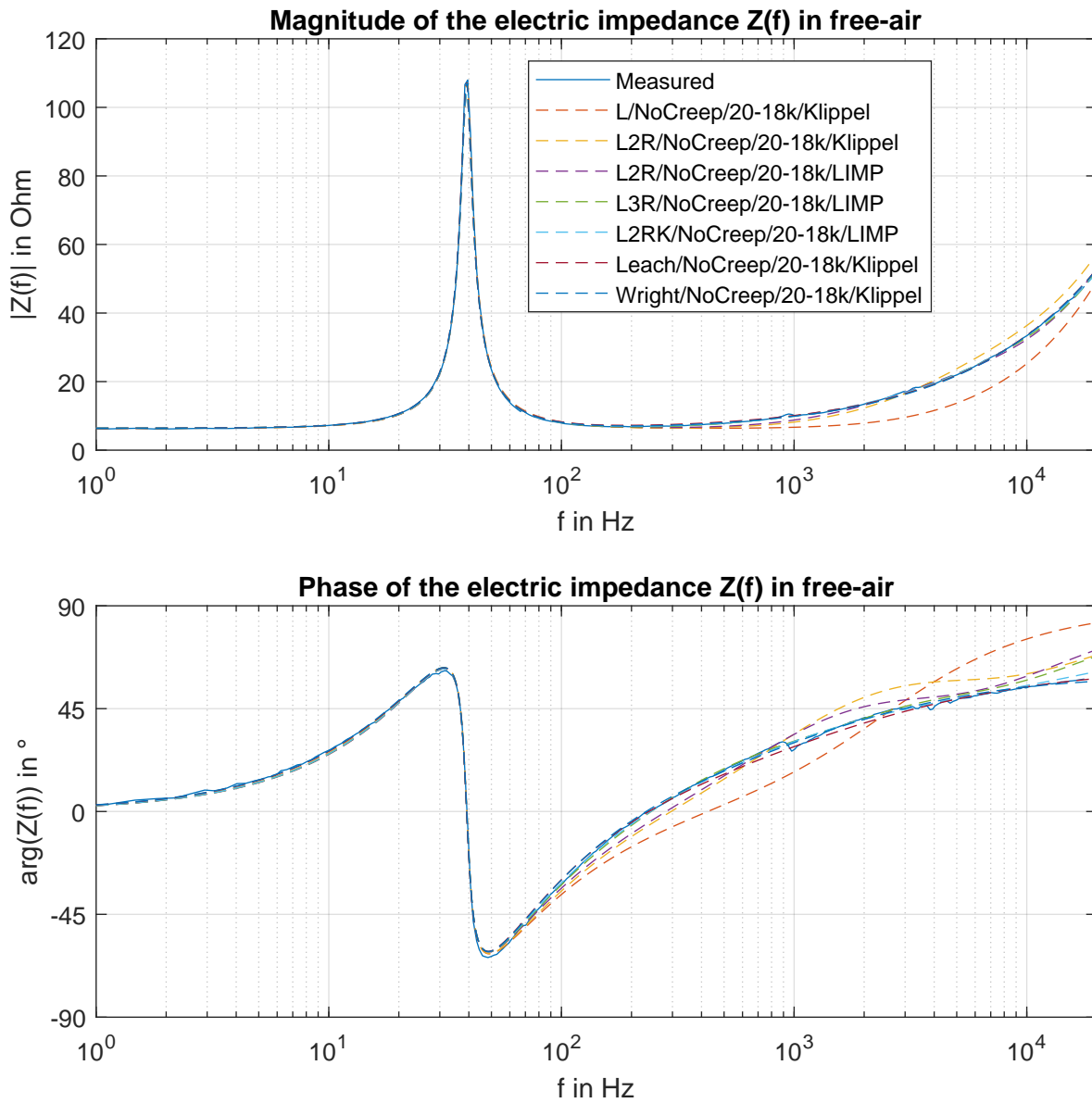


Figure 4.3: Comparison of the measured impedance with the simulated impedance using different voice coil models in free air

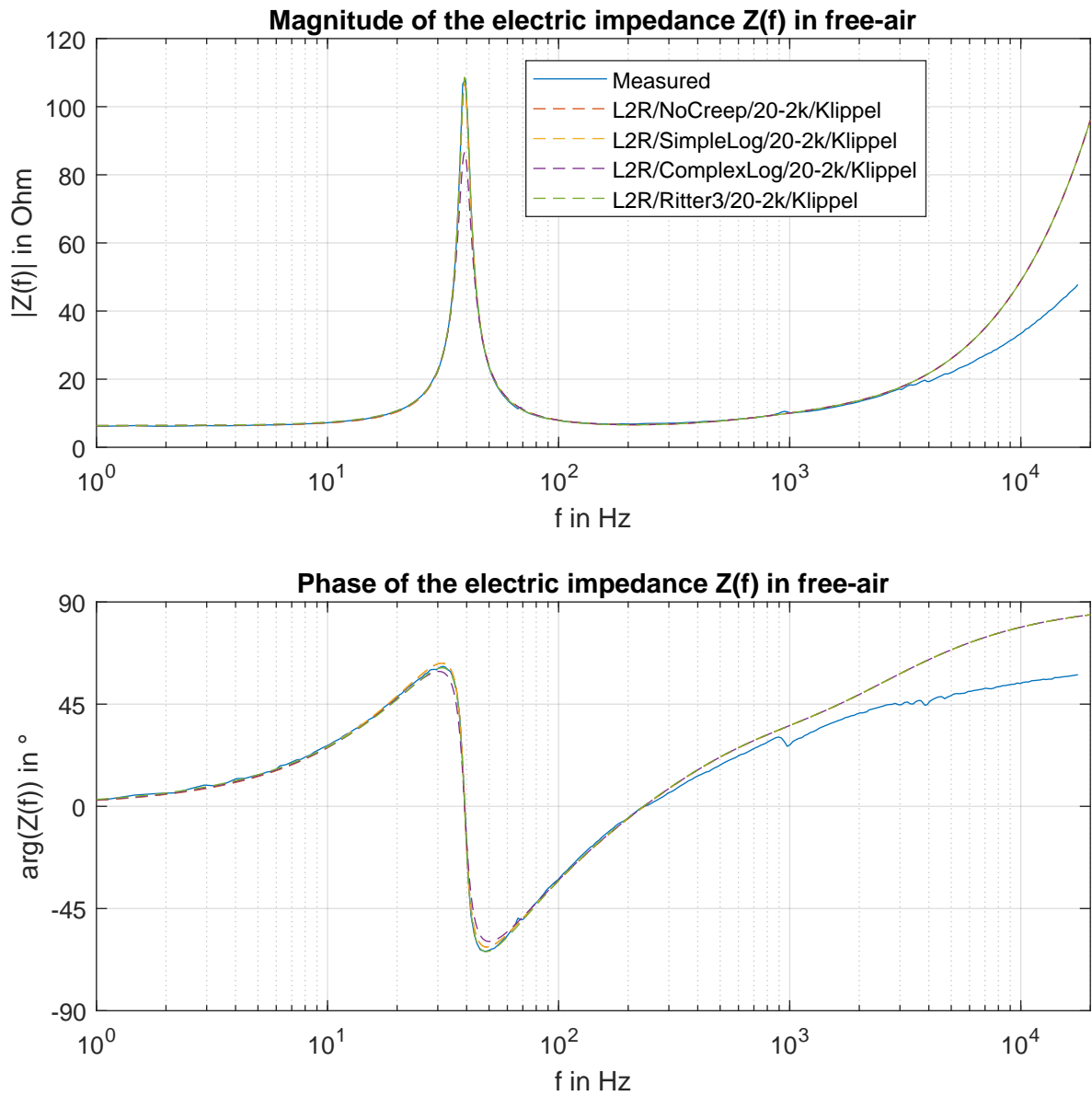


Figure 4.4: Comparison of the measured impedance with the simulated impedance using different creep models in free air

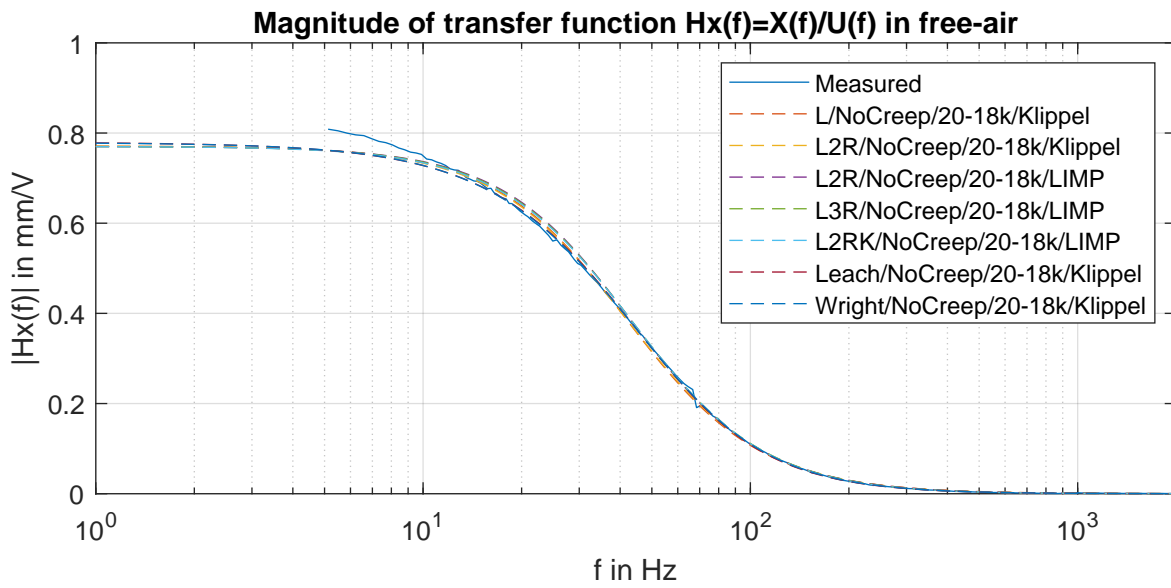


Figure 4.5: Comparison of the measured displacement with the simulated displacement using different voice coil models in free air

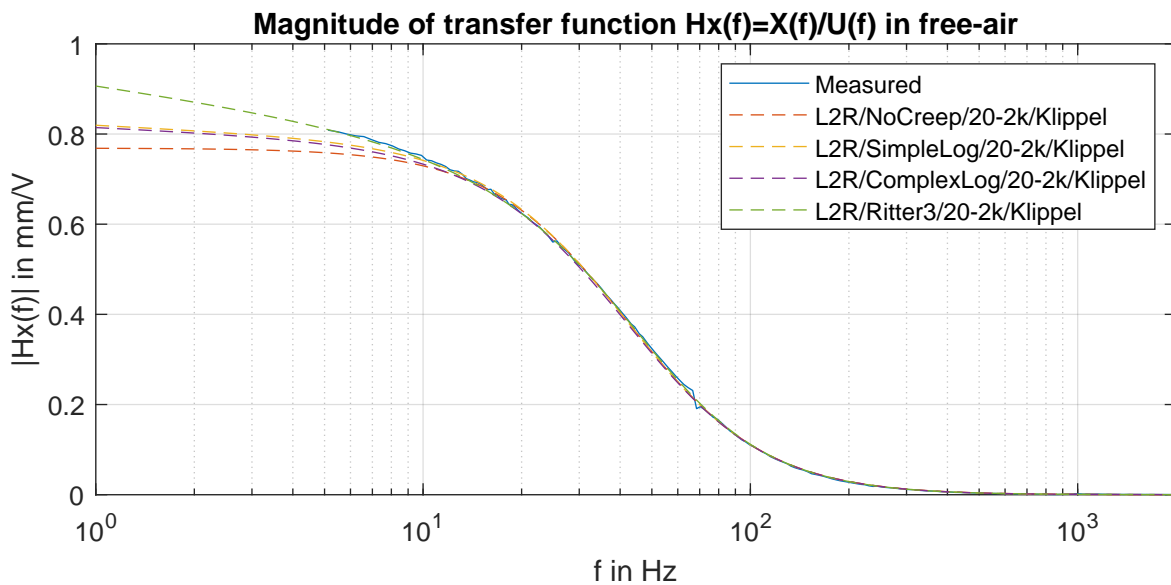


Figure 4.6: Comparison of the measured displacement with the simulated displacement using different creep models in free air

Model	Error $e$ in %	
	$(f = 5 \dots 18\,000 \text{ Hz})$	
	Impedance	
	Magnitude	Phase
L/NoCreep/20-18k/Klippel	3.5809	7.7209
L2R/NoCreep/20-18k/Klippel	0.4335	1.8707
L2R/NoCreep/20-18k/LIMP	0.1669	0.8917
L3R/NoCreep/20-18k/LIMP	0.1132	0.2612
L2RK/NoCreep/20-18k/LIMP	0.1054	0.0878
Leach/NoCreep/20-18k/Klippel	0.0675	0.1386
Wright/NoCreep/20-18k/Klippel	0.0579	0.0906

Table 4.5: Deviation between the measured and the modelled impedance in free air between 5 Hz and 18 kHz

Model	Error $e$ in %		
	$(f = 5 \dots 2000 \text{ Hz})$		
	Impedance		Displacement
Magnitude	Phase		
L/NoCreep/20-18k/Klippel	0.8398	5.7526	0.0722
L2R/NoCreep/20-18k/Klippel	0.2406	1.2874	0.0679
L2R/NoCreep/20-18k/LIMP	0.2569	0.7698	0.0942
L3R/NoCreep/20-18k/LIMP	0.1821	0.1212	0.0882
L2RK/NoCreep/20-18k/LIMP	0.1818	0.1203	0.0839
Leach/NoCreep/20-18k/Klippel	0.1035	0.2091	0.0693
Wright/NoCreep/20-18k/Klippel	0.0802	0.1314	0.0670
L2R/NoCreep/20-2k/Klippel	0.0759	0.7584	0.0730
L2R/SimpleLog/20-2k/Klippel	0.0726	0.7583	0.0261
L2R/ComplexLog/20-2k/Klippel	1.8363	0.9612	0.0456
L2R/Ritter3/20-2k/Klippel	0.0511	0.7556	0.0063

Table 4.6: Deviation between the measured and the modelled impedance and displacement in free air between 5 Hz and 2 kHz

## 5

## Simulation Program

The software *Speaker Analyzer 2.2* [14] has been used for modelling the behaviour of a dynamic loudspeaker. It is based on the *Speaker Analyzer 2.1* [15] by Florian Loacker-Schöch and the most important changes leading to *Speaker Analyzer 2.2* are the following.

- Models for the voice coil have been implemented as described in chapter 2 on page 2. That means the chain matrix  $\mathbf{A}_1$  from [16, eq. 5.6] is updated to

$$\mathbf{A}_1 = \begin{bmatrix} 1 & R_E + \frac{Z_{LE}(\omega)}{1} \\ 0 & 1 \end{bmatrix}. \quad (5.1)$$

The selection of the voice coil model is only supported when using the *Extended Model* setting.

- Models that account for the creep of the suspension have been implemented as described in chapter 3 on page 9. That means the chain matrix  $\mathbf{A}_3$  from [16, eq. 5.11] is updated to

$$\mathbf{A}_3 = \begin{bmatrix} 1 & 0 \\ R_{m,Ma} + j\omega m_{Mk} + \frac{1}{j\omega C(\omega)} & 1 \end{bmatrix}. \quad (5.2)$$

Suspension creep models are only supported when using the *Extended Model* setting.

- The performance has been improved by using less frequency points (1000 instead of 20 000) but with an improved spacing (logarithmic instead of linear).
- Functionality has been added so curves are also exported to a MAT-file.
- Functionality has been added so the transfer function  $H_x(\omega) = \frac{x(\omega)}{U_G}$  is also exported when exporting the displacement of the membrane.
- The software has been translated to English.
- References to the underlying equations have been partially added within the code and the documentation of some functions have been improved.

The source code and the full list of changes can be found under [https://gitlab.com/faymann/speaker\\_analyzer](https://gitlab.com/faymann/speaker_analyzer).

Using one of the voice coil models or suspension creep models does come with the restriction that the *Normalized Sound Pressure Level*, *Impulse Response*, *Step Response* and *Group Delay* tabs are not available, except when using the L2R or L3R voice coil model.

A screenshot of the application can be seen in figure 5.1 on the facing page. The additional controls for the voice coil modeling and suspension creep modeling are highlighted. The following sections give a brief summary about the various model parameters and how to obtain them.

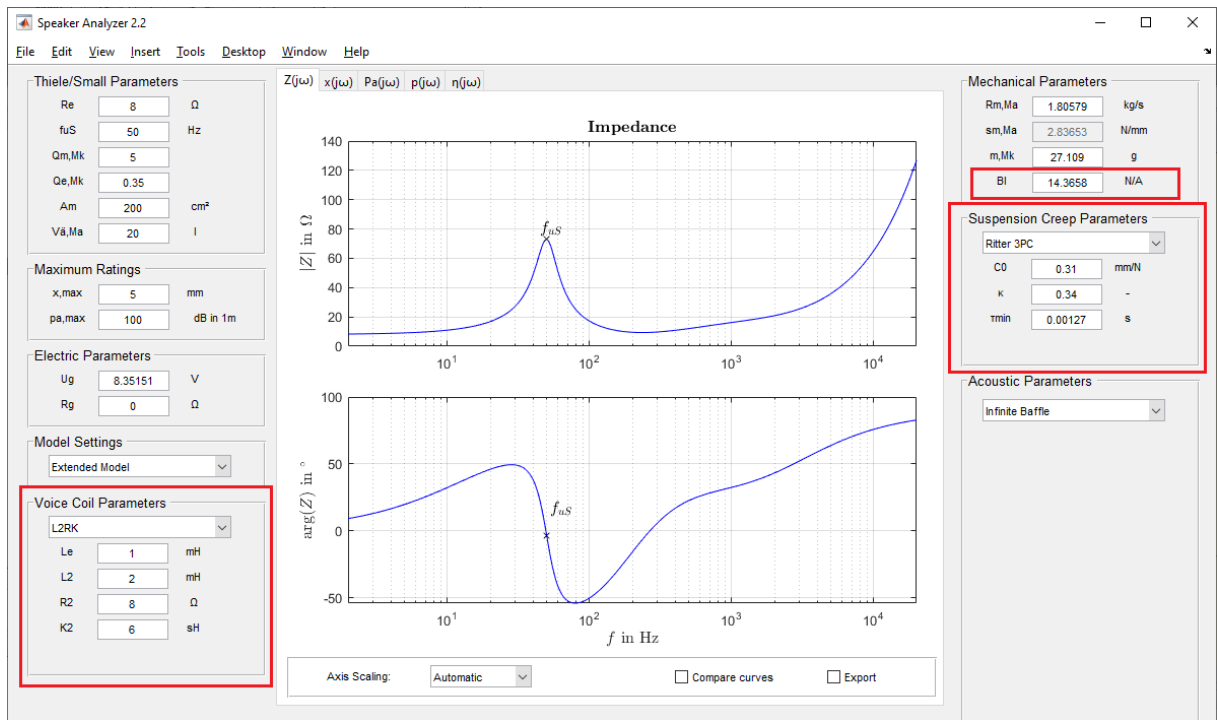


Figure 5.1: Screenshot of the Speaker Analyzer 2.2 with the added controls highlighted

## 5.1 Voice Coil Parameters

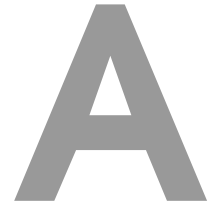
Model	Parameters	Formula	Parameters can be obtained using
L2R	$L_E, L_2, R_2$	2.1 on page 2	LIMP [5, p. 32] and Klippel [10, p. 24]. In Klippel the model is called <i>LR-2</i> .
L3R	$L_E, L_2, R_2, L_3, R_3$	2.3 on page 3	LIMP [5, p. 32].
L2RK	$L_E, L_2, R_2, K_2$	2.5 on page 5	LIMP [5, p. 32].
Leach	$K, n$	2.8 on page 7	Klippel [10, p. 24].
Wright	$K_r, E_r, K_x, E_x$	2.11 on page 8	Klippel [10, p. 24]. The parameters are called slightly different.

## 5.2 Suspension Creep Parameters

Model	Parameters	Formula	Parameters can be obtained using
SLS	$C_0, C_1, \eta_1$	3.6 on page 10	-
Ritter 3P	$C_0, \kappa, \tau_{min}$	3.40 on page 17	Klippel [11, p. 4] in combination with the formula 3.43 on page 18. In Klippel the model is called <i>Ritter</i> .
Ritter 4P	$C_0, \kappa, \tau_{min}, \tau_{max}$	3.44 on page 18	-
Simple Log	$C_0, \lambda$	3.16 on page 14	Klippel [11, p. 2] in combination with the formulas 3.13 on page 13 and 3.14 on page 13. In Klippel the model is called <i>Log</i> .
Complex Log	$C_0, \lambda$	3.10 on page 12	Klippel [11, p. 3] in combination with the formulas 3.13 on page 13 and 3.14 on page 13. In Klippel the model is called <i>Knudsen</i> .

## Bibliography

- [1] F. Agerkvist, K. Thorborg, und C. Tinggard, „A Study of the Creep Effect in Loudspeaker Suspension,” in *Audio Engineering Society Convention 125*, Oct 2008. [Online]. Available: <http://www.aes.org/e-lib/browse.cfm?elib=14713>
- [2] F. T. Agerkvist und T. Ritter, „Modeling Viscoelasticity of Loudspeaker Suspensions Using Retardation Spectra,” in *Audio Engineering Society Convention 129*, Nov 2010. [Online]. Available: <http://www.aes.org/e-lib/browse.cfm?elib=15639>
- [3] W. Klippel, „Tutorial: Loudspeaker Nonlinearities—Causes, Parameters, Symptoms,” *J. Audio Eng. Soc.*, Vol. 54, Nr. 10, S. 907–939, 2006. [Online]. Available: <http://www.aes.org/e-lib/browse.cfm?elib=13881>
- [4] F. Loacker-Schöch, „Elektroakustische Modellbildung und Optimierung von Lautsprechersystemen,” 2018. [Online]. Available: <https://www.spsc.tugraz.at/student-projects/elektroakustische-modellbildung-und-optimierung-von-lautsprechersystemen.html>
- [5] I. Mateljan, *LIMP User Manual*, Artalabs, J. Rodina 4, 21215 Kastel Luksic, Croatia, Nov 2019.
- [6] I. Mateljan und M. Sikora, „Estimation of loudspeaker driver parameters,” in *Proc. of 5th Congress of the Alps Adria Acoustics Association*, 2012. [Online]. Available: <http://www.aes.org/e-lib/browse.cfm?elib=15639>
- [7] M. Dodd, W. Klippel, und J. Ocle-Brown, „Voice Coil Impedance as a Function of Frequency and Displacement,” in *Audio Engineering Society Convention 117*, Oct 2004. [Online]. Available: <http://www.aes.org/e-lib/browse.cfm?elib=12835>
- [8] W. M. Leach, Jr., „Loudspeaker Voice-Coil Inductance Losses: Circuit Models, Parameter Estimation, and Effect on Frequency Response,” *J. Audio Eng. Soc.*, Vol. 50, Nr. 6, S. 442–450, 2002. [Online]. Available: <http://www.aes.org/e-lib/browse.cfm?elib=11074>
- [9] J. R. Wright, „An Empirical Model for Loudspeaker Motor Impedance,” *J. Audio Eng. Soc.*, Vol. 38, Nr. 10, S. 749–754, 1990. [Online]. Available: <http://www.aes.org/e-lib/browse.cfm?elib=6011>
- [10] *Linear Parameter Measurement*, Klippel R&D SYSTEM, Mendelssohnallee 30, 01309 Dresden, Germany, Nov 2020.
- [11] *Extended Creep Modeling*, Klippel R&D SYSTEM, Mendelssohnallee 30, 01309 Dresden, Germany, Jun 2013.
- [12] M. H. Knudsen und J. G. Jensen, „Low-Frequency Loudspeaker Models That Include Suspension Creep,” *J. Audio Eng. Soc.*, Vol. 41, Nr. 1/2, S. 3–18, 1993. [Online]. Available: <http://www.aes.org/e-lib/browse.cfm?elib=7015>
- [13] J. D. Ferry, *Viscoelastic Properties of Polymers*, 3. Aufl. John Wiley & Sons, 1980.
- [14] M. Faymann, „Speaker Analyzer 2.2.” [Online]. Available: [https://gitlab.com/faymann/speaker\\_analyzer](https://gitlab.com/faymann/speaker_analyzer)
- [15] F. Loacker-Schöch, „Speaker Analyzer 2.1.” [Online]. Available: [https://gitlab.com/florian\\_ls/speaker\\_analyzer](https://gitlab.com/florian_ls/speaker_analyzer)
- [16] —, „Realisierung eines modularen Lautsprechersystems,” 2020.



## Measurement data and source code

The measurement data as well as the source code should come along with the documentation. If not, please contact the author or supervisor of the presented master project.

Table A.1 lists all Matlab scripts that have been used for processing the measurement data and creating the diagrams, in addition to the *Speaker Analyzer 2.2*. The corresponding Matlab functions are listed in table A.2 on the next page.

Script name	Description
<code>script_compliance_diagram</code>	The script which creates the diagrams for chapter 3 on page 9.
<code>script_klippel_to_limp</code>	The script which merges the measurement data from Klippel and converts it into a data format that can be processed by LIMP.
<code>script_main</code>	The script which creates the diagrams for chapter 4 on page 20 and computes the squared errors in percent.
<code>script_voice_coil_diagrams</code>	The script which creates the diagrams for chapter 2 on page 2.

Table A.1: Matlab scripts

Function name	Description
<code>compute_error</code>	A function which computes the squared error in percent between the measured and the simulated impedance and displacement in free-air. The measured impedance, the measured displacement and the loudspeaker parameters have to be supplied.
<code>compute_fq</code>	A function which computes the resonance frequency and mechanical and electrical quality factors from the magnitude of an impedance measurement.
<code>compute_impedance_displacement</code>	A function which computes the total impedance and displacement of a loudspeaker in free-air using the specified loudspeaker parameters.
<code>compute_knudsen_from_klippel</code>	A function which computes $C_0$ and $\lambda$ from $\tilde{C}_0$ and $\tilde{\lambda}$ using the equations 3.13 on page 13 and 3.14 on page 13.

<code>convert_klippel_to_limp</code>	A function which converts the impedance data from a m-file created by Klippel to a file that can be read by LIMP.
<code>export_figure</code>	A function which creates a PDF-file from a Matlab figure.
<code>load_curve</code>	A function which loads a curve from an m-file created by Klippel.
<code>load_parameters</code>	A function which loads loudspeaker parameters from an m-file.
<code>merge_curve</code>	A function which combines two spectra using a cross-over frequency.
<code>merge_klippel</code>	A function which combines two impedance and displacement measurements using a cross-over frequency.
<code>plot_impedance_displacement</code>	A function which creates impedance and displacements plots for a loudspeaker in free-air. It loads the measurement data, loads the loudspeaker parameters, performs the simulation, computes the squared errors in percent and plots and exports the results.
<code>save_curve</code>	A function which creates an m-file from a spectrum.
<code>trim_curve</code>	A function which reduces the number of frequency points of a spectrum.
<code>trim_curve_file</code>	A function which reduces the number of frequency points of a spectrum stored in an m-file.

---

*Table A.2: Matlab functions*